The area of high radiation technologies on the basis of the accelerator complex NICA (suggestions for implementation)

S.Tyutyunnikov
Joint Institute for Nuclear Research, Dubna, Russia

1997, Belovezhskaya Pushcha

Kurchatov synchrotron radiation source, 1999

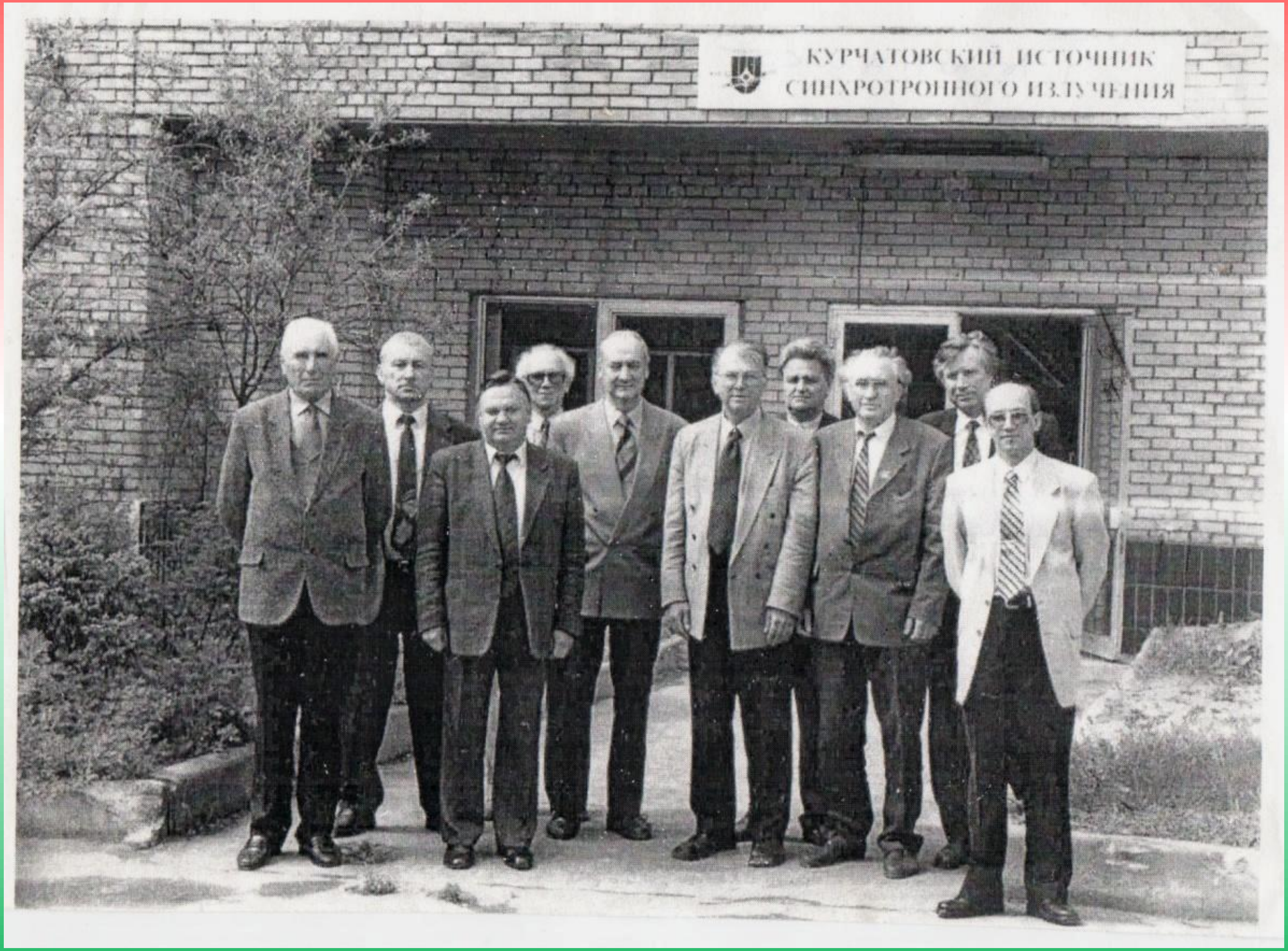

Contents:

Various Applications of the KEK AIA

- Warm Dense Matter Science
- Nanostructure Fabrication (Ion Track, Nanowire)
- Ion-tuning to Make Intelligent Material & Surface Improvement
- Hybrid Cancer Therapy with H, C and Fe
- Mutation Breeding
- Micro-beam for Biological Science
- SEU Experiments for Microprocessor, Semiconductor & Power Transistor

Simulation of cosmic particle radiation using high-energy accelerators

E = 100 – 2000 MeV/u

SIS-18 FAIR
GANIL SPIRAL2
HIMAC

1. Radiobiological risk assessment for manned space missions

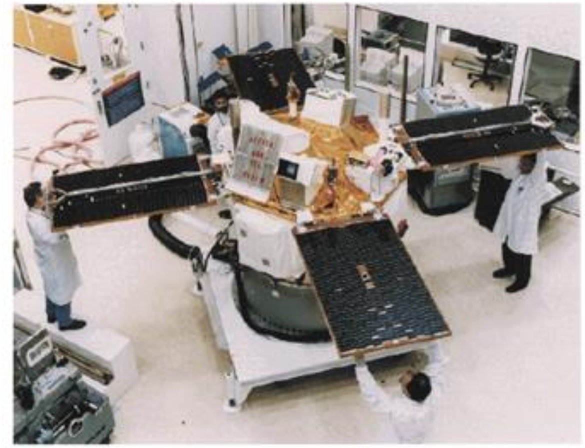

2. Test and calibration of space flight instruments

NASA Space Radiation Lab
Brookhaven

3. Radiation hardness tests

High-energy ion beams for space research

High-Energy Irradiation Facility for High-Energy Irradiation Facility for Biophysics and Material Research - BIOMAT

Research program: Space radiation effects

- heavy ion induced modifications of soliids under extremely high pressure
- analysis of material modifications induced by relativistic heavy ions
-Radiation hardness of materials

Equipments:

- Magnetic scanner system
- Flexible irradiation set-ups
- Instrumentation for in-situ diagnostics of irradiated samples

BIOMAT Research Fields

Biophysics

Cosmic radiation: the main hindrance toward manned space exploration

Widely unknown biological effects of heavy ions

NASA and ESA started a large experimental campaign in space radiation biophysics

Particle Therapy

Materials Research

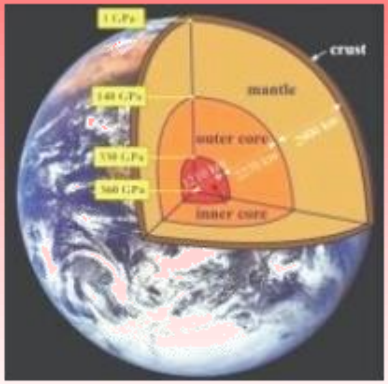

Radiation effects under high pressure: phase transitions in mineralogy and geophysics

Ion-matter interaction at relativistic beam energies: energy-deposition and short-time processes

Radiation hardness of materials: requirements for accelerator and spacecraft-components

Warm Dense Matter Science and Material Creation

Sample Region
Extreme High Pressure < 100 Gpa
=> High Density
Warm

High-energy ions

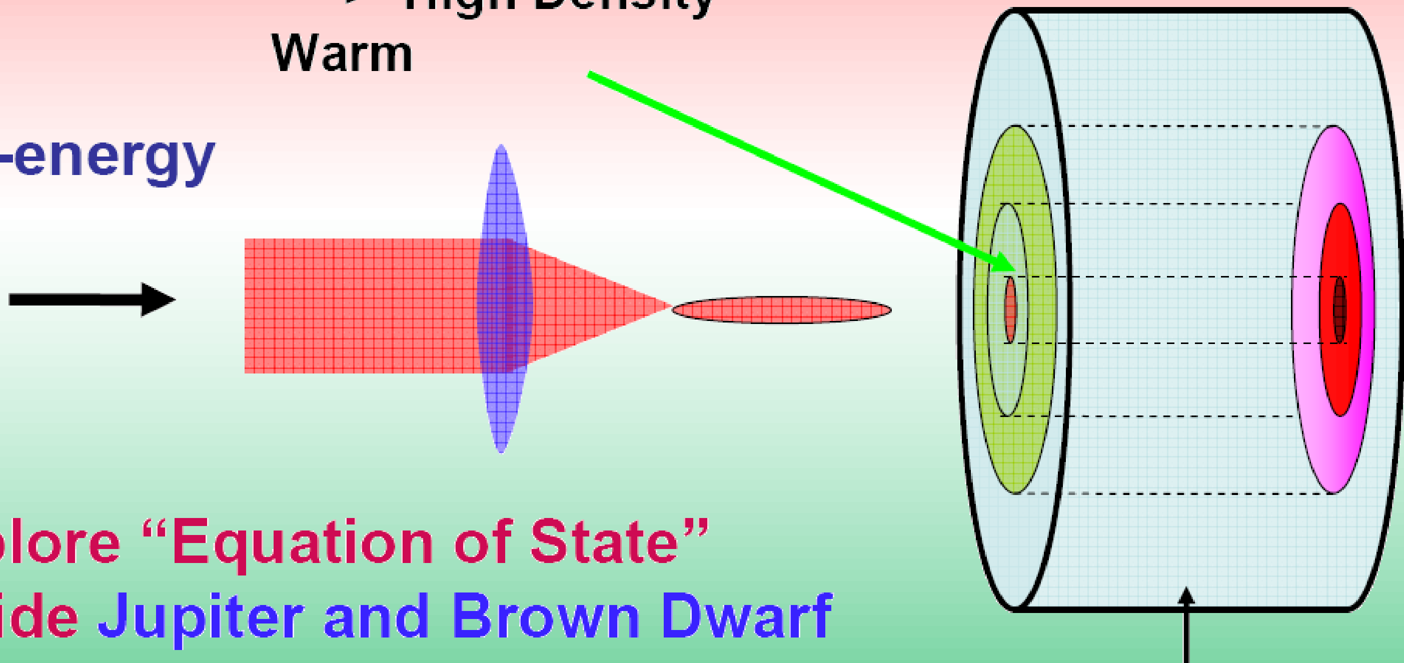

Pb or Ta tamper

explore "Equation of State"
inside Jupiter and Brown Dwarf

Radiation damage of electronic components

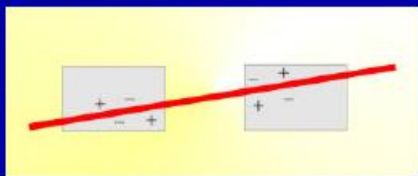

Single energetic particles may cause malfunctioning of microelectronic devices
SEU = Single Event Upset
SEL Latch-up
e.g. Bit-Flip in Storage-Chips

Results of GSI beam times (AMS-Collaboration)

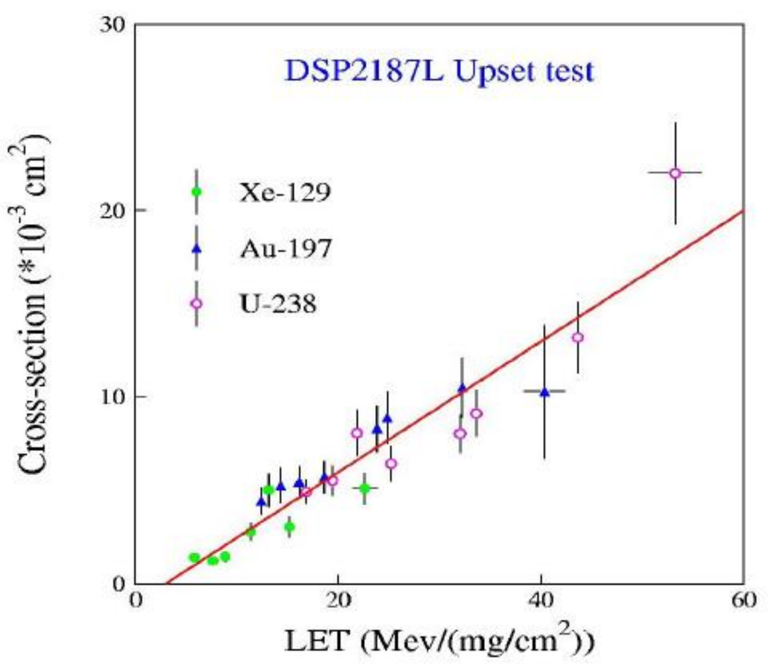

Table 2: Estimate of SEE rates per component on ISS.

Component	Part Number	SEL rate (day^{-1})	SEU rate (day^{-1})
DSP	ADSP2187L	$8 \cdot 10^{-8}$	$1 \cdot 10^{-4}$
DSP	ADSP2189M	$2 \cdot 10^{-7}$	$2 \cdot 10^{-4}$
DALLAS controller	DS80C390	$2 \cdot 10^{-3}$	
CPU	PPC750	$3 \cdot 10^{-13}$	-
Host/PCI bridge	CPC700	$1 \cdot 10^{-10}$	-
PCI Adaptor	PLX PCI9080	$1 \cdot 10^{-3}$	-
Watchdog Timer	AMD679	$5 \cdot 10^{-9}$	$4 \cdot 10^{-8}$
CPLD	CY3700	$2 \cdot 10^{-12}$	$3 \cdot 10^{-5}$
SDRAM 128 Mbit	MT48LC8M16A2	$1 \cdot 10^{-11}$	$3 \cdot 10^{-3}$
FLASH memory	MBM29DL324TE	$1 \cdot 10^{-8}$	$3 \cdot 10^{-7}$
HV controller	MHV100	$2 \cdot 10^{-6}$	$1 \cdot 10^{-4}$
PGA	QL12X16BL	$3 \cdot 10^{-7}$	$5 \cdot 10^{-8}$
PGA	Actel 54SX32	$4 \cdot 10^{-13}$	$3 \cdot 10^{-9}$
RICH FE chip	AMS	$4 \cdot 10^{-8}$	$8 \cdot 10^{-8}$
ECAL FE chip	AMS	negl	-
HCC	AMS	$2 \cdot 10^{-7}$	negl
Digital Coupler	ISO150	negl	$5 \cdot 10^{-4}$
Digital Coupler	ADM	$6 \cdot 10^{-9}$	negl
ADC	ADS803U	$3 \cdot 10^{-9}$	$2 \cdot 10^{-7}$
VA32 old		$1 \cdot 10^{-6}$	-
VA32 new		$2 \cdot 10^{-8}$	-

Radiation load for space flights

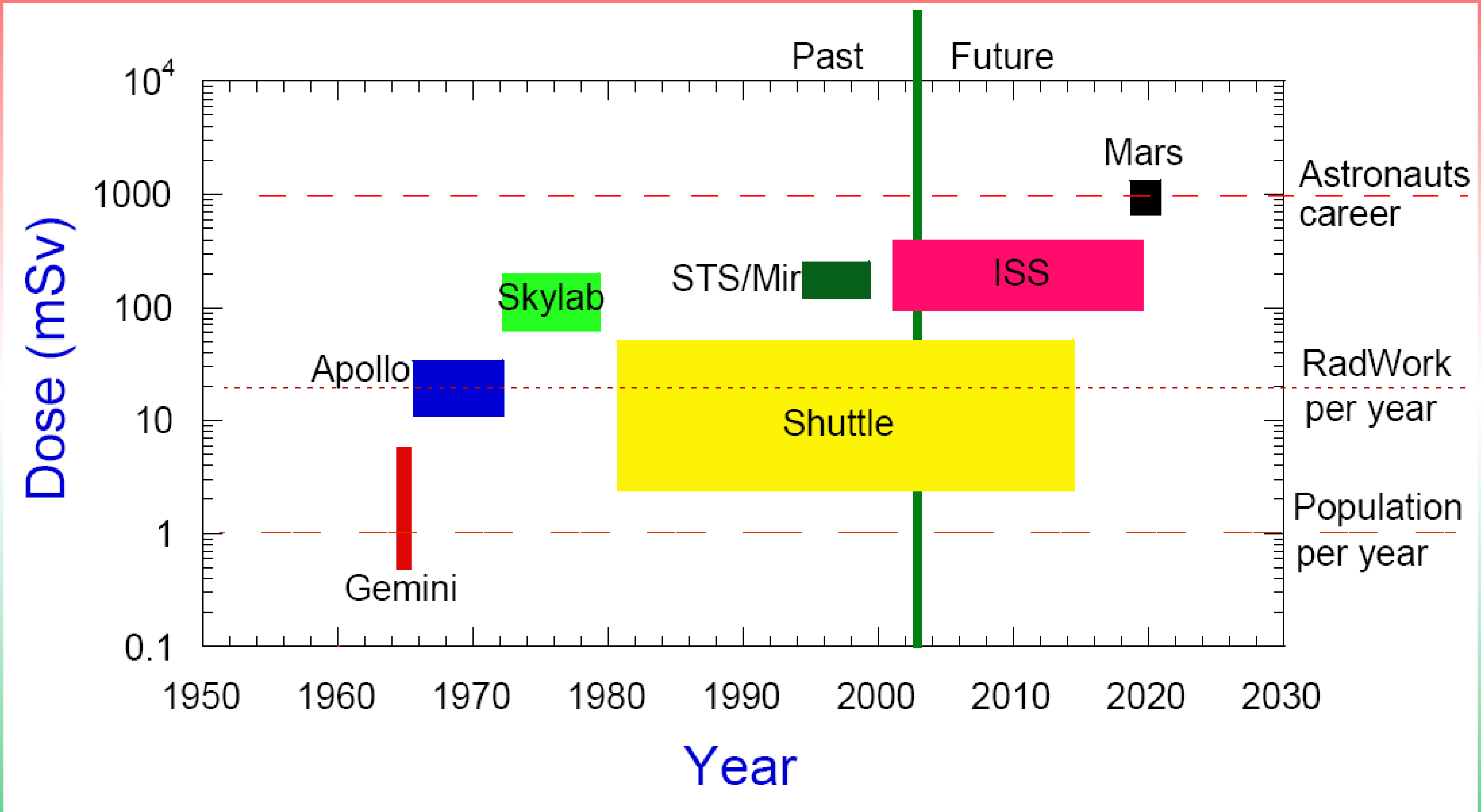

The damage induced by heavy ions

Damage induction after heavy ion irradiation

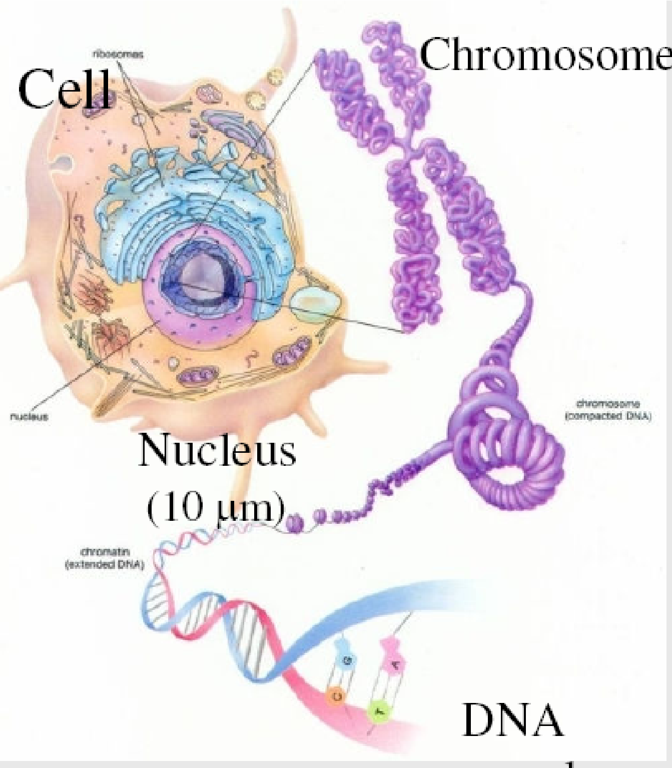

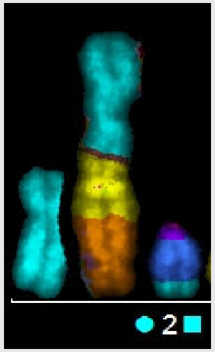

Hartel et al. (2009)
Radiother. Oncol.

Mutation
Chromosomal
aberration

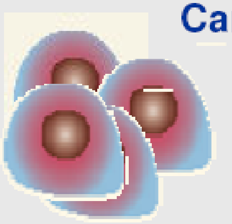

Cancer

More smaller fragments (AFM)
Psonka-Antonyzk et al. (2009)
Radiat. Res.
⇒ **Impaired DSB repair**

Multiple lesions
in close proximity

clustered damage

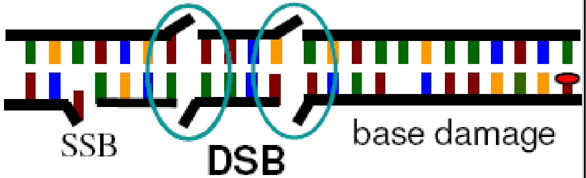

M. Krämer

Microbeam irradiation for biological and medical science

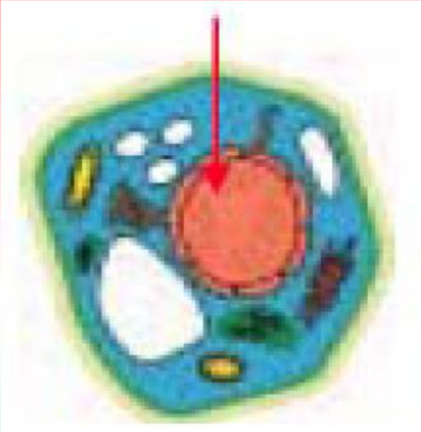

Aiming at part of Chromosome in cell

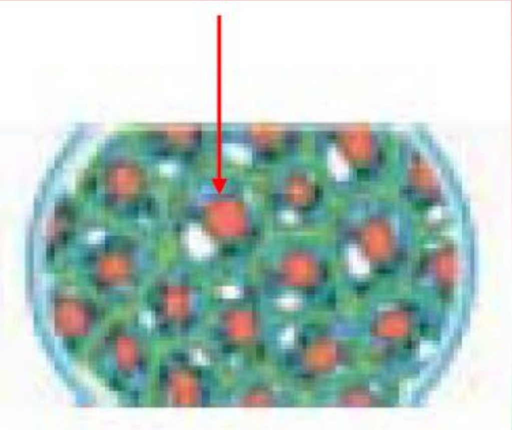

Aiming at one cell in cell block

The main directions of scientific-methodical and innovative work on the beams of relativistic nuclei

1. Radiocarbon Therapy: A prototype of the complex for radiocarbon therapy
2. Creation of complex equipment for radiobiological studies to simulating galactic radiation
3. Radiation Materials science :
   - Radiation damage of micro electronics
   - Technology for creating electronic structures in the tracks of relativistic ions

Microbeams of heavy ions for research of local damage in cells

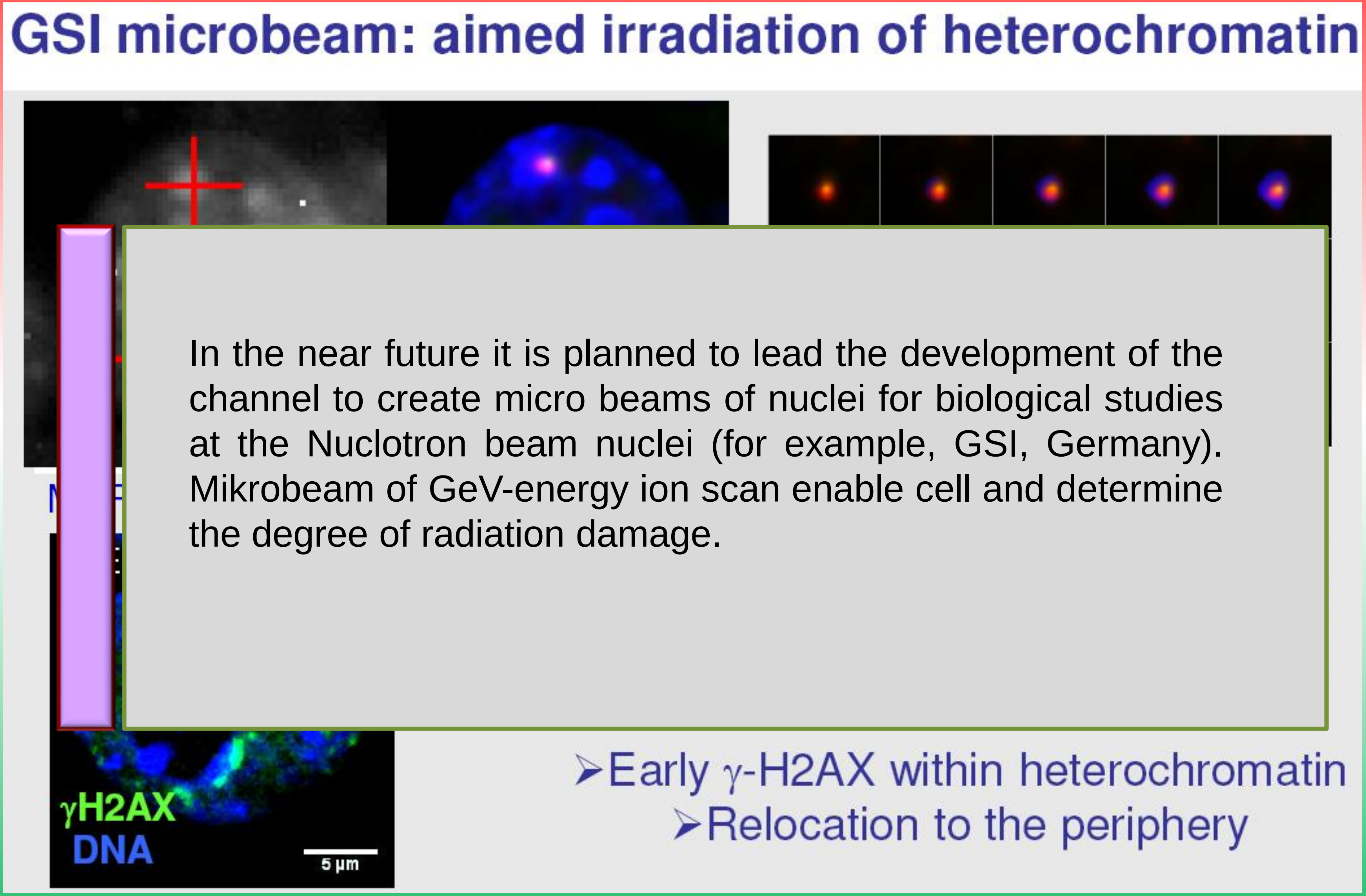

In the near future it is planned to lead the development of the channel to create micro beams of nuclei for biological studies at the Nuclotron beam nuclei (for example, GSI, Germany). Mikrobeam of GeV-energy ion scan enable cell and determine the degree of radiation damage.

Superconducting accelerator complex NICA
(Nuclotron based Ion Collider fAcility)

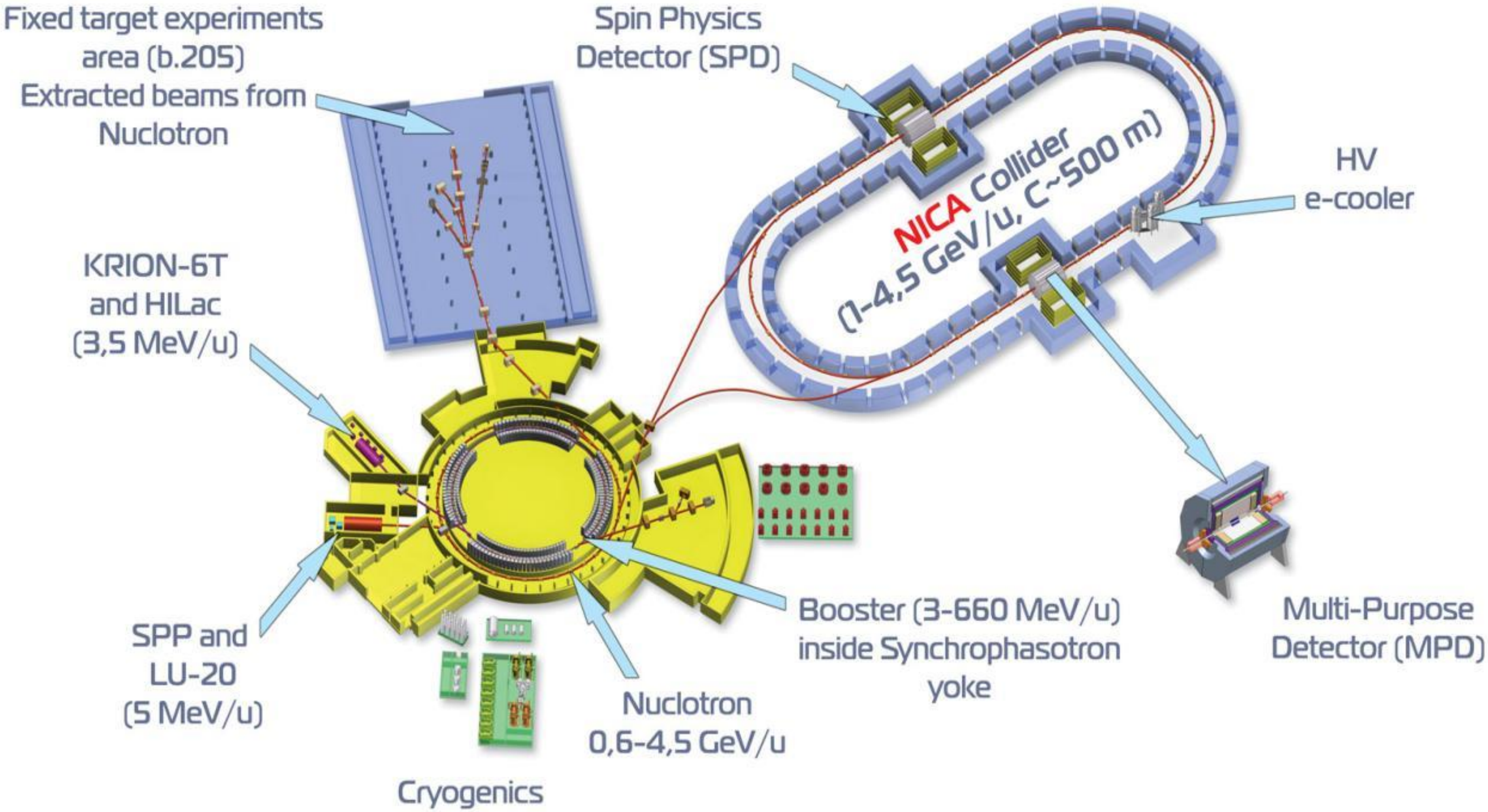

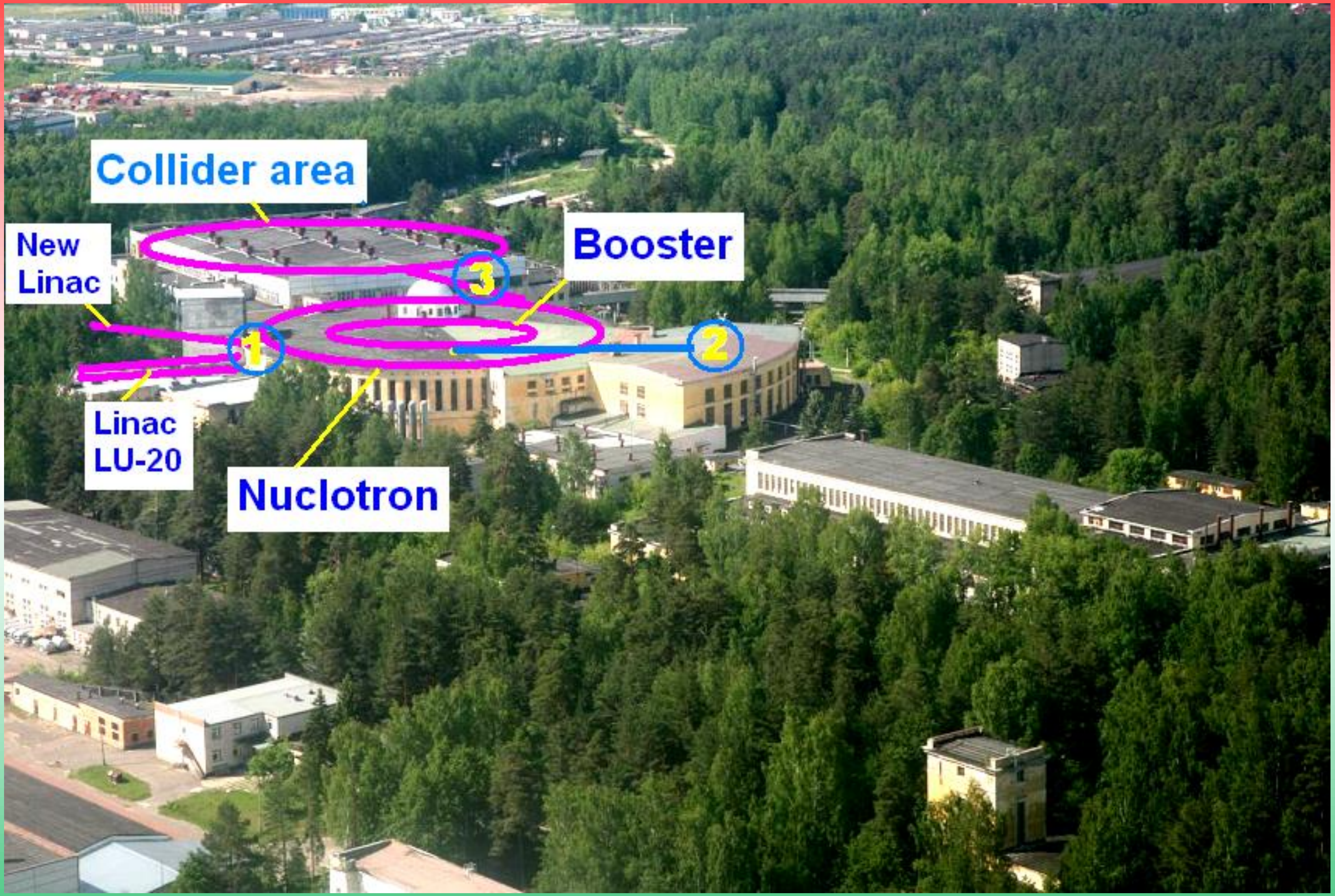
Collider area
New Linac
Booster
3
1
2
Linac LU-20
Nuclotron

NICA scheme

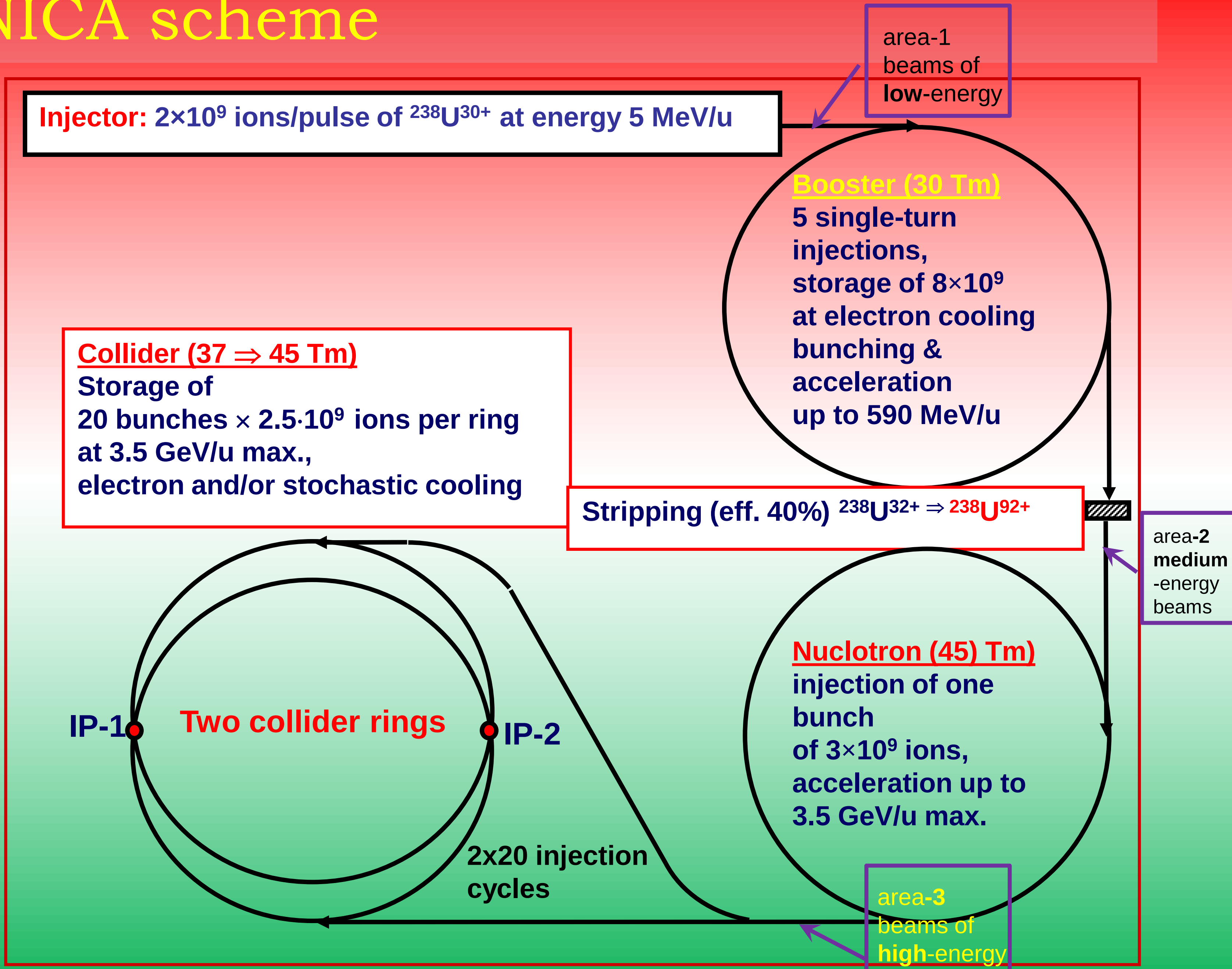
area-1
beams of
low-energy
Injector: 2×10⁹ ions/pulse of ²³⁸U³⁰⁺ at energy 5 MeV/u
Booster (30 Tm)
5 single-turn injections,
storage of 8×10⁹
at electron cooling
bunching &
acceleration
up to 590 MeV/u
Collider (37 ⇒ 45 Tm)
Storage of
20 bunches × 2.5·10⁹ ions per ring
at 3.5 GeV/u max.,
electron and/or stochastic cooling
Stripping (eff. 40%) ²³⁸U³²⁺ ⇒ ²³⁸U⁹²⁺
area-2
medium
-energy
beams
IP-1
Two collider rings
IP-2
Nuclotron (45) Tm)
injection of one bunch
of 3×10⁹ ions,
acceleration up to
3.5 GeV/u max.
2x20 injection
cycles
area-3
beams of
high-energy

The existing accelerator complex VBLHEP

Intensity nucl/cycl		
beam	recd	future
p,d	$5 \cdot 10^{10}$	10^{13}
^{4}He	10^7	10^9
^{12}C	$2 \cdot 10^9$	$7 \cdot 10^9$
^{24}Mg	10^8	$3 \cdot 10^8$
^{56}Fe	10^6	10^7
^{84}Kr	10^4	$2 \cdot 10^7$
^{124}Xe	10^4	10^6

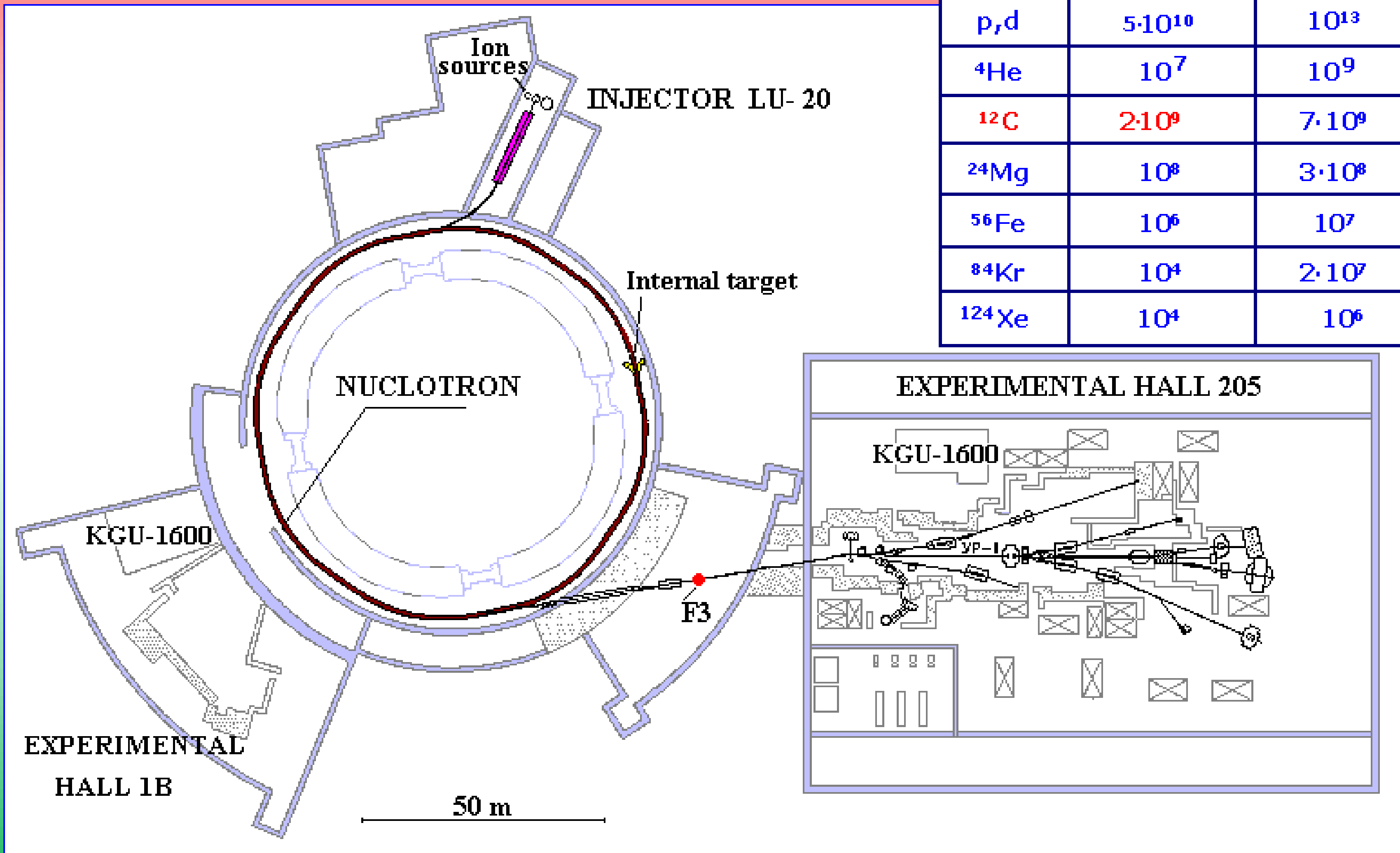

Experimental areas for BIOMAT research

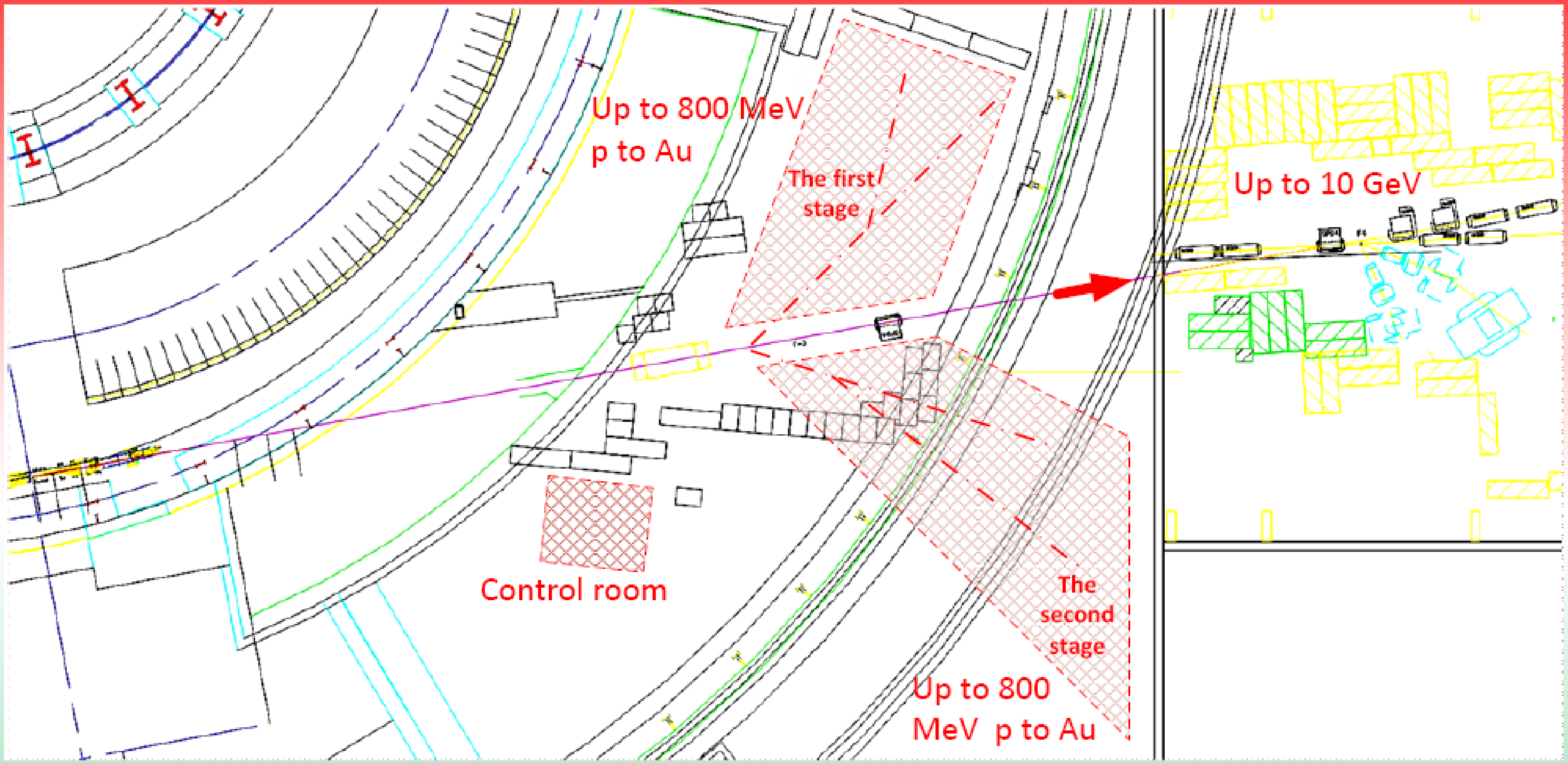

The first – the experimental setup at the gallery for the irradiation of electronics for space equipment's, materials and biological objects

The second - the radiobiology research to application of carbon therapy including of proton microscope for visualization of area irradiation

The third – the radiobiology researches on influence the high energy up to 10 GeV/u of protons and heavy ions on biological samples

Using beams of the NICA

area-**1** beams of low-energy	area-**2** medium-energy beams	area-**3** beams of high-energy
Planned nanotechnology researches based into injector **NICA**	The study of radiation damage microelectronic component radiobiological research (space program) Research in material science Development of the prototype units Complex of Carbon Radiotherapy	The study of radiation damage microelectronic component Radiobiological research (space program) Relativistic Nuclear Energetics ◆ Generation of thermal power ◆ Disposal of nuclear waste ◆ Remote control of fissile materials

Projects under the theme of 1107 for the 2017-2019 years.

Energy &Transmutation

- Setup Quinta - Nuclotron extracted beam (205 VBLHEP building);
- Simulation of hybrid nuclear reactor on the basis of a deep subcritical assembly of natural uranium, excited by a beam of high-energy ions. Research possibility of transmutation of radioactive waste under the influence of radiation.
- Setup “Big uranium target" - extracted beam from Phazotron (LNP);
- Studying the effects of coherent electromagnetic radiation in the beta decay of long-lived isotopes (IR laser, FEM millimeter range - 42 VBLHEP building). The interested member country - Poland, the Russian Federation.

Radiated Materials Science

Studying of influence of powerful beam of particles and electromagnetic radiation on semiconductor and superconducting materials

- Radiation resistance of classic and high-temperature superconductors - extracted beam from LNP Phasotron;
- Effect of large doses of high-energy ions (Nuclotron extracted beam, BM & N channel), high energy electrons and hard X-rays (LIA-3000, 42 build. VBLHEP) on Semiconducting micro-devices (customer - Zelenograd).

The development of physical methods of nuclear medicine

Methods of destruction of cancerous tumors under the influence of light ions beams and coherent electromagnetic radiation in conditions of tissue saturation by nanoscale absorbers of radiation

- A prototype of oxygen therapy channel with the additional influence of microwave radiation (booster VBLHEP extracted beam);
- Study of the possibilities of proton therapy with the additional influence of microwave radiation (medical channel of LNP Phasotron);
- The impact of coherent electromagnetic radiation on cancer cells in the tissue saturation conditions by nanoscale absorbers (IR laser, FEM millimeter range - 42 VBLHEP building). The interested member country – Belarus.

Study of irradiation of sub-critical uranium assembly + lead target. International collaboration “Energy+Transmutation” at **Nuclotron**

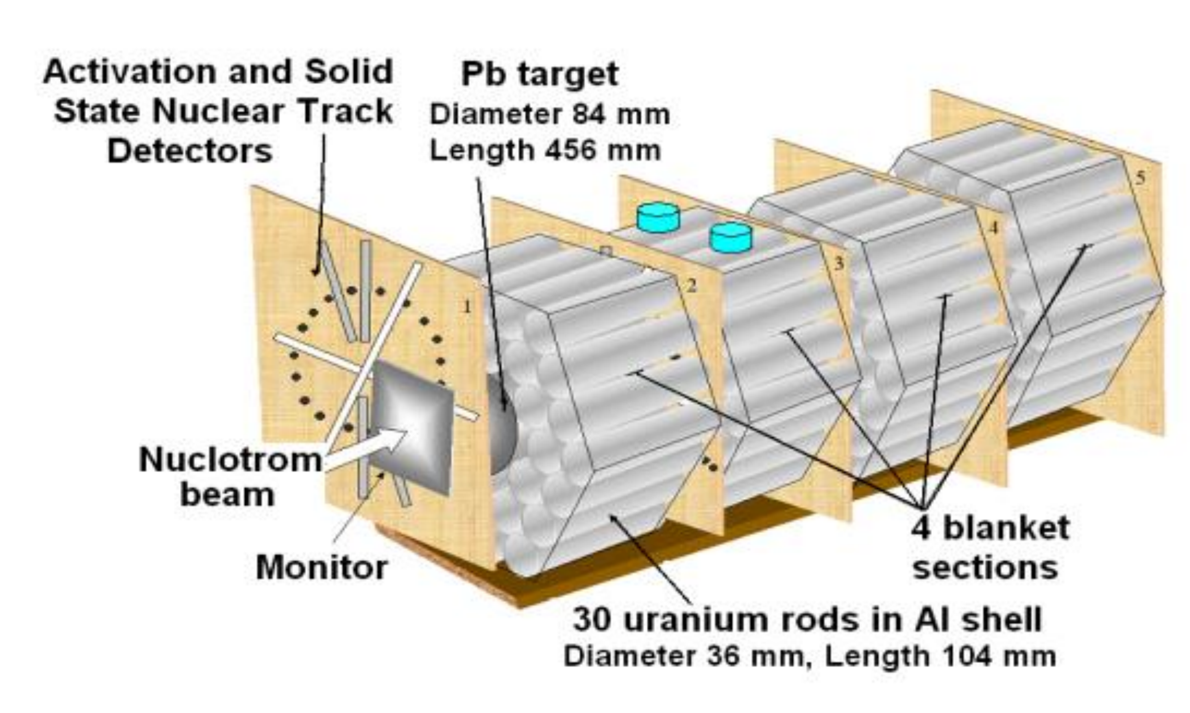

Getting new basic nuclear-physics data with relativistic proton, deutron and light ion beams **(1 - 4.5 GeV/n)**
for modeling and design of the active core of the prototype for close-to-industrial setup of the radioactive waste processing

Mass of uranium – *19.5 т.* *Materials of central zone* – *U, Th, Pb.*
Diameter – *1,2 м.* *Diameter of central zone* – *0,2 м.*
Length – *1 м.*

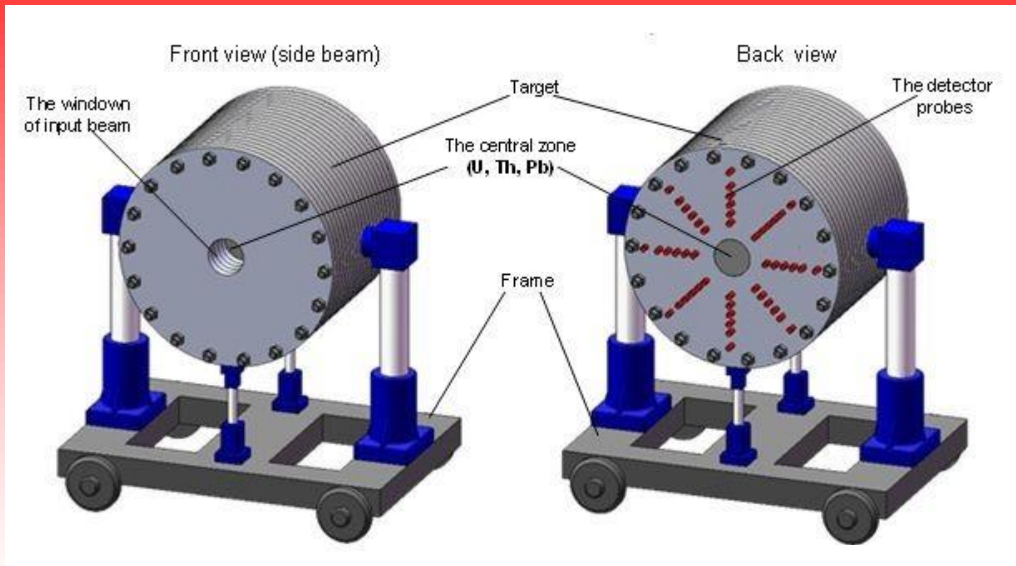

General view of the target setup BURAN at the transport-fixing platform.

The scheme of longitudinal section of the TS BURAN with the mounted central zone (top-left) and general view photo (right).

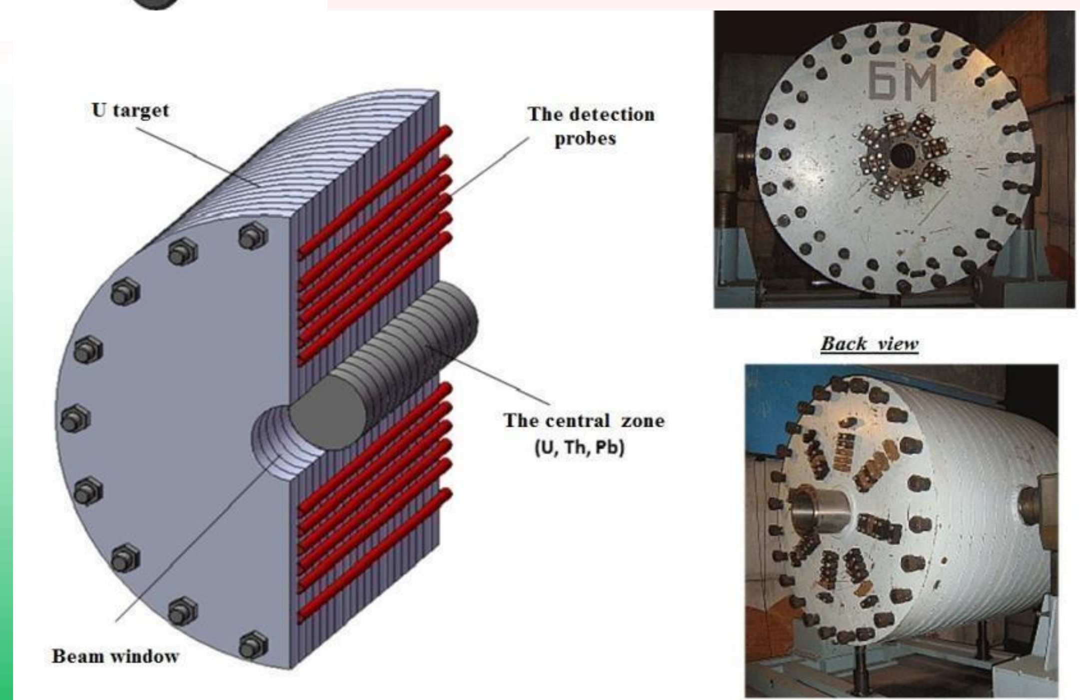

Energy multiplication in the target

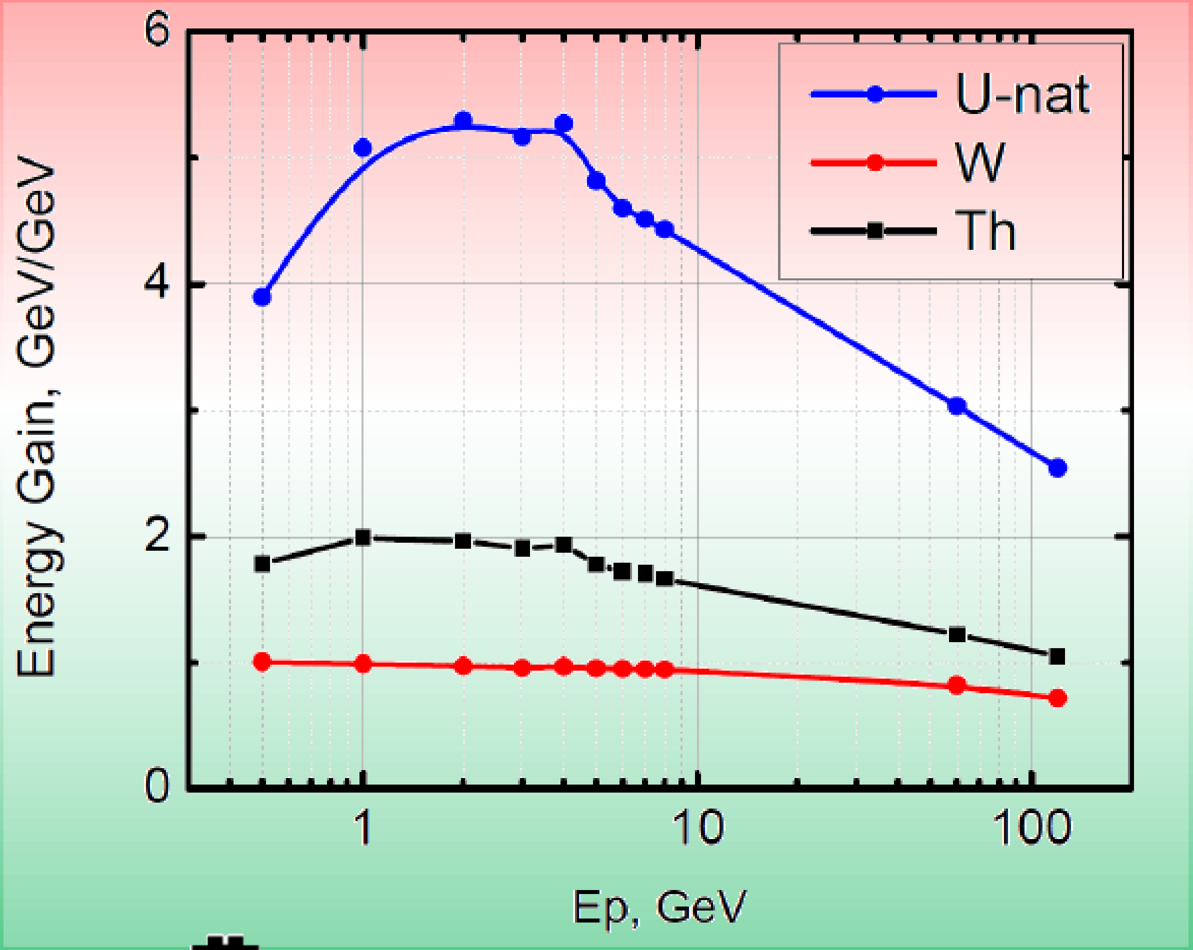

Fermilab

Fermilab-Conf-14-177-APC-TD

June 2014

Cosmic Ray Composition and Spectra

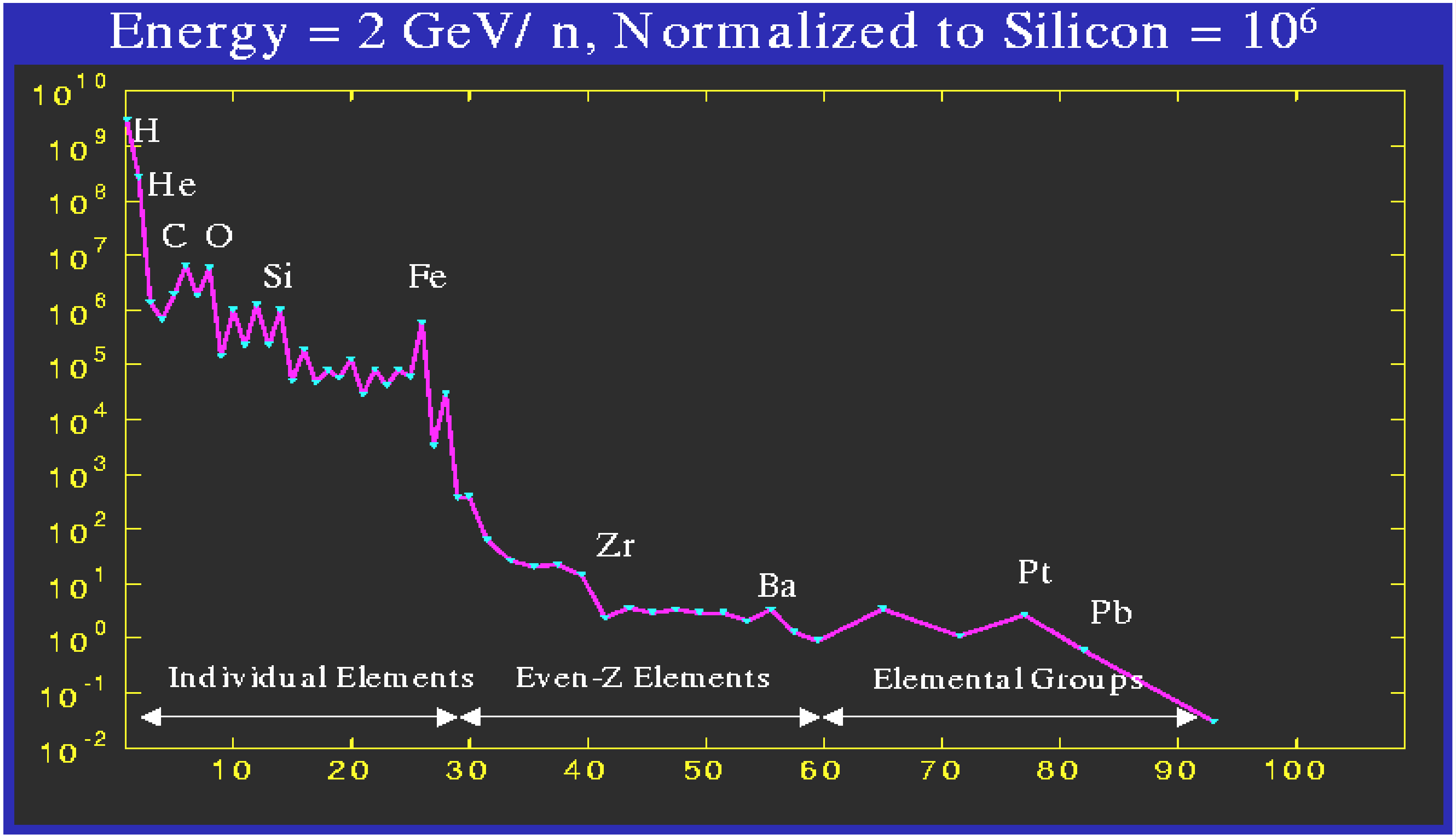

ISO 15390 standard: Galactic Cosmic Ray model (Nymmik, MSU) e.g. in CREME-96

Radiation damage of electronic components. Experiments at the Nuclotron.

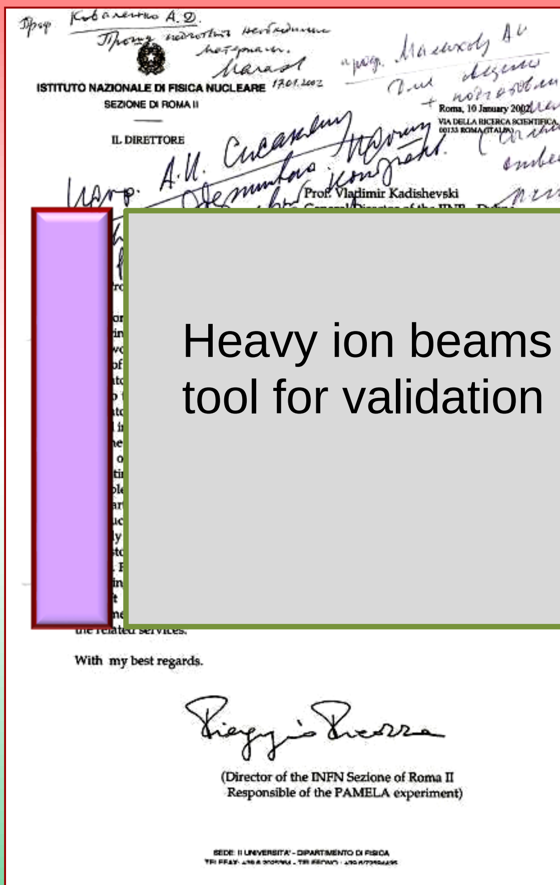

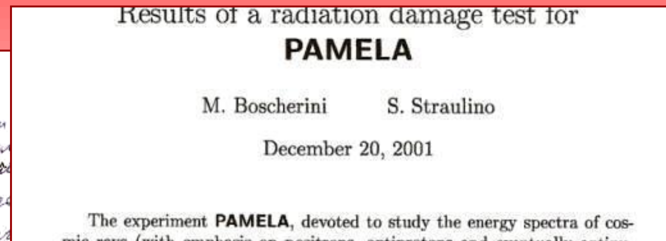

Results of a radiation damage test for

PAMELA

M. Boscherini S. Straulino

December 20, 2001

The experiment **PAMELA**, devoted to study the energy spectra of cosmic rays (with emphasis on positrons, antiprotons and eventually antinu-

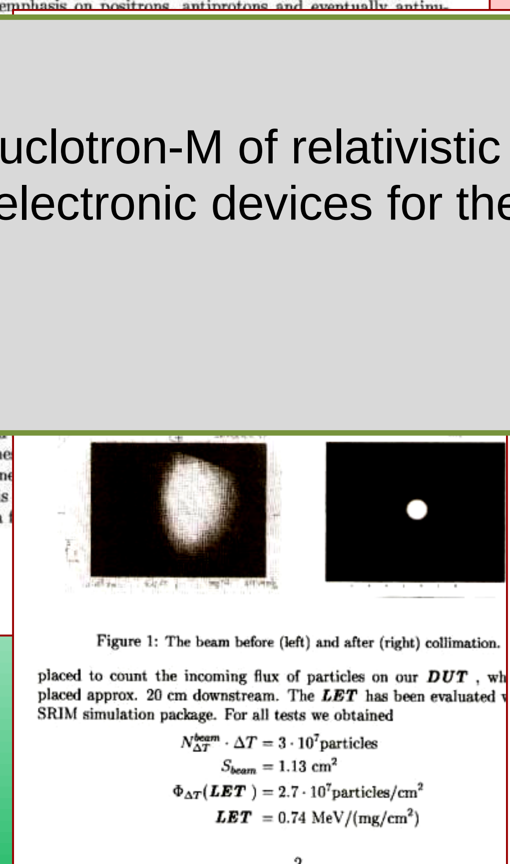

Figure 1: The beam before (left) and after (right) collimation.

placed to count the incoming flux of particles on our ***DUT*** , wh placed approx. 20 cm downstream. The ***LET*** has been evaluated SRIM simulation package. For all tests we obtained

$$N^{beam}_{\Delta T} \cdot \Delta T = 3 \cdot 10^7 \text{particles}$$
$$S_{beam} = 1.13\ \text{cm}^2$$
$$\Phi_{\Delta T}(LET) = 2.7 \cdot 10^7 \text{particles/cm}^2$$
$$LET = 0.74\ \text{MeV/(mg/cm}^2)$$

2

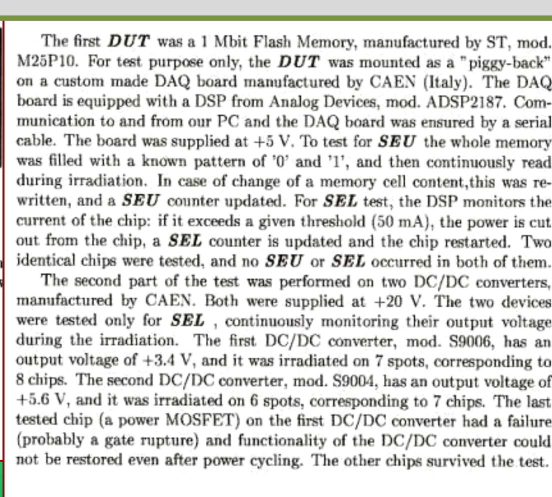

The first ***DUT*** was a 1 Mbit Flash Memory, manufactured by ST, mod. M25P10. For test purpose only, the ***DUT*** was mounted as a "piggy-back" on a custom made DAQ board manufactured by CAEN (Italy). The DAQ board is equipped with a DSP from Analog Devices, mod. ADSP2187. Communication to and from our PC and the DAQ board was ensured by a serial cable. The board was supplied at +5 V. To test for ***SEU*** the whole memory was filled with a known pattern of '0' and '1', and then continuously read during irradiation. In case of change of a memory cell content,this was rewritten, and a ***SEU*** counter updated. For ***SEL*** test, the DSP monitors the current of the chip: if it exceeds a given threshold (50 mA), the power is cut out from the chip, a ***SEL*** counter is updated and the chip restarted. Two identical chips were tested, and no ***SEU*** or ***SEL*** occurred in both of them.

The second part of the test was performed on two DC/DC converters, manufactured by CAEN. Both were supplied at +20 V. The two devices were tested only for ***SEL*** , continuously monitoring their output voltage during the irradiation. The first DC/DC converter, mod. S9006, has an output voltage of +3.4 V, and it was irradiated on 7 spots, corresponding to 8 chips. The second DC/DC converter, mod. S9004, has an output voltage of +5.6 V, and it was irradiated on 6 spots, corresponding to 7 chips. The last tested chip (a power MOSFET) on the first DC/DC converter had a failure (probably a gate rupture) and functionality of the DC/DC converter could not be restored even after power cycling. The other chips survived the test.

Heavy ion beams of the Nuclotron-M of relativistic energies are an unique tool for validation of microelectronic devices for the space program

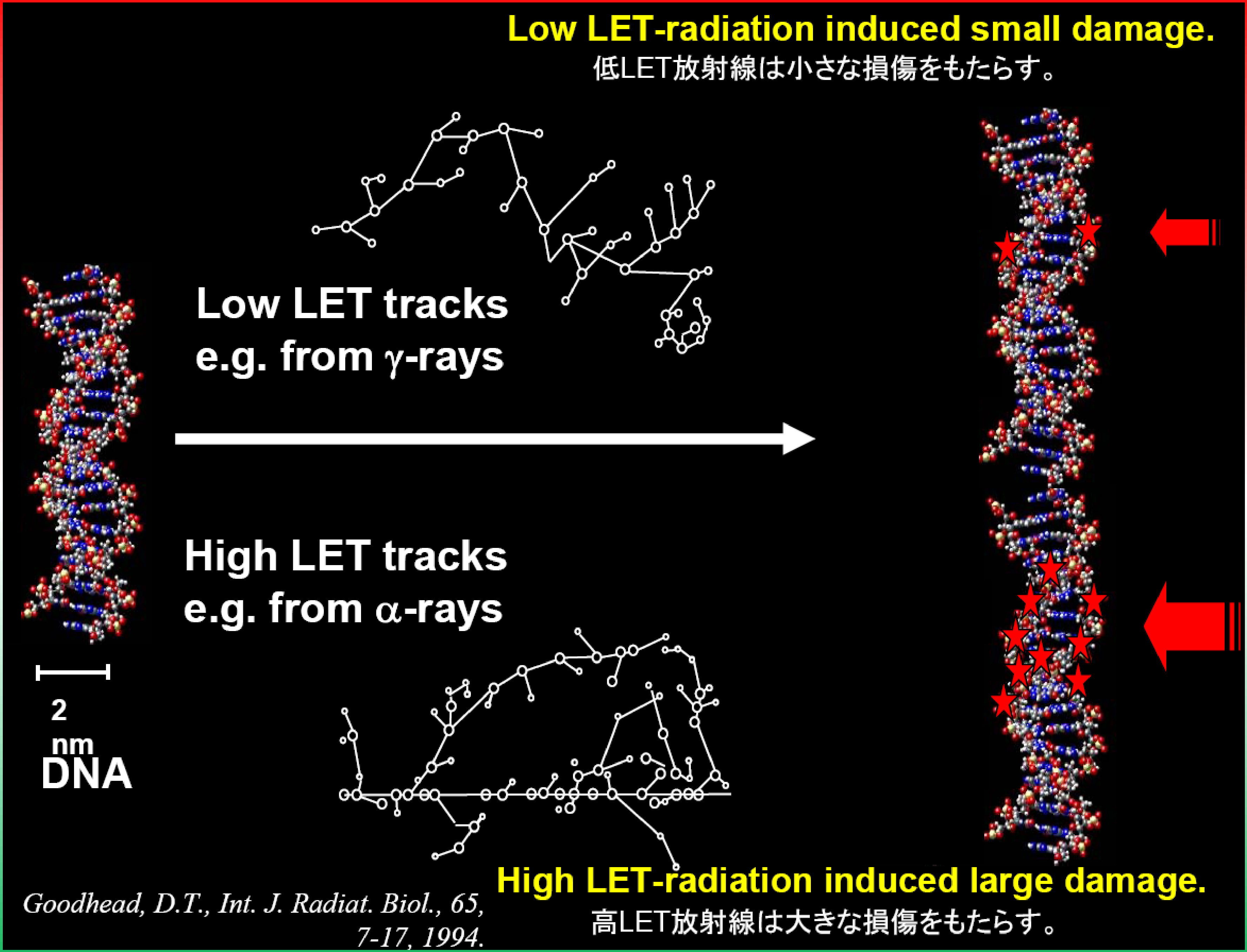
Low LET-radiation induced small damage.
低LET放射線は小さな損傷をもたらす。
Low LET tracks
e.g. from γ-rays
High LET tracks
e.g. from α-rays
2
nm
DNA
High LET-radiation induced large damage.
高LET放射線は大きな損傷をもたらす。
Goodhead, D.T., Int. J. Radiat. Biol., 65, 7-17, 1994.

LET 線エネルギー付与 Linear energy transfer

High LET α-ray β-ray
Neutron, Heavy particles

Low LET X-ray γ-ray

RBE 生物効果比 Relative biological effectiveness

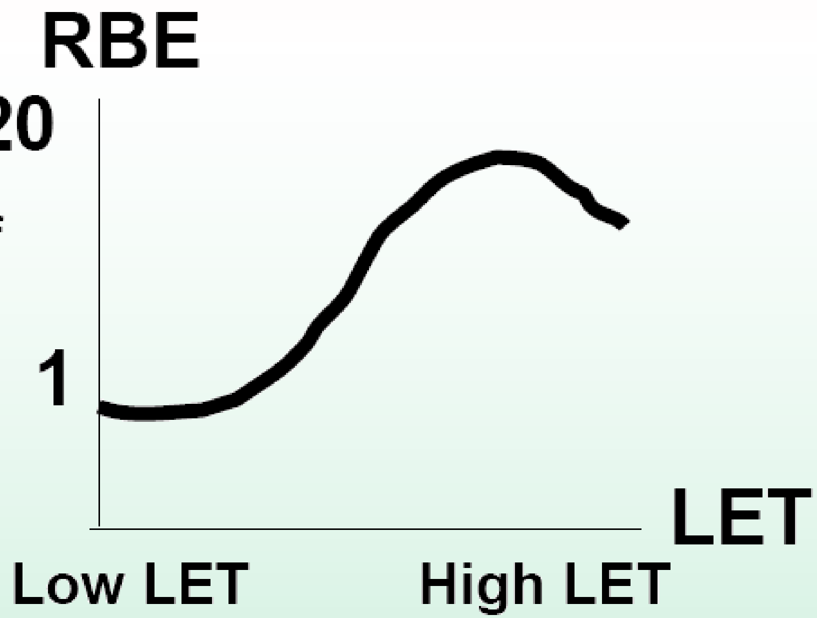

We should study about RBE of high LET-radiations.

Carcinogenesis

Cancer therapy

Space radiations

Live cell imaging of heavy ion traversals in euchromatin and heterochromatin

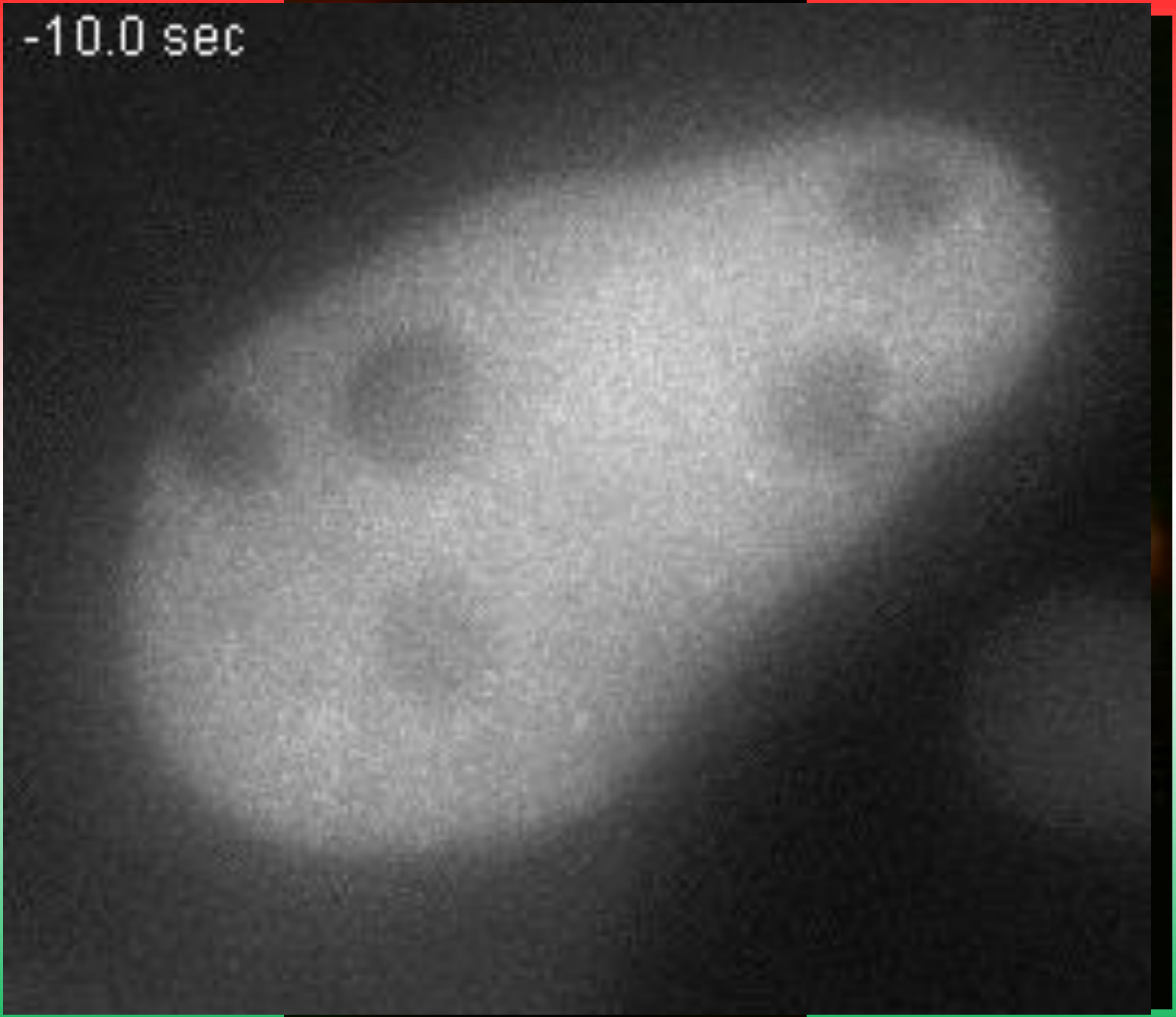

Jakob *et al., Proc. Natl. Acad. Sci. USA* 2009; *Nucl. Acids Res*. 2011

Why are we interested in energetic heavy ions?

^{1}H to ^{56}Fe
100-10000 MeV/n

^{1}H to ^{20}Ne
70-400 MeV/n

Heavy ion radiation is not present naturally on Earth

PHYSICAL SUPPORT OF RADIOBIOLOGICAL EXPERIMENTS AT NUCLOTRON

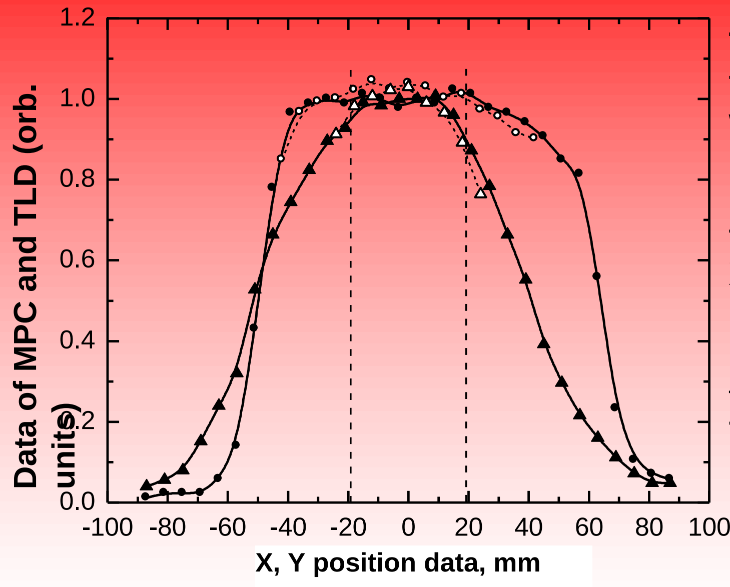

The spatial distributions of X and Y wires currents measured by the multiwire proportional chamber (● – X; ▲–Y) and TLD readings distribution (○ –X; Δ – Y) in the formed field of 1 GeV protons. The dashed lines are the borders of the irradia-tion area

The quasiuniform particle field is formed in biological patterns area

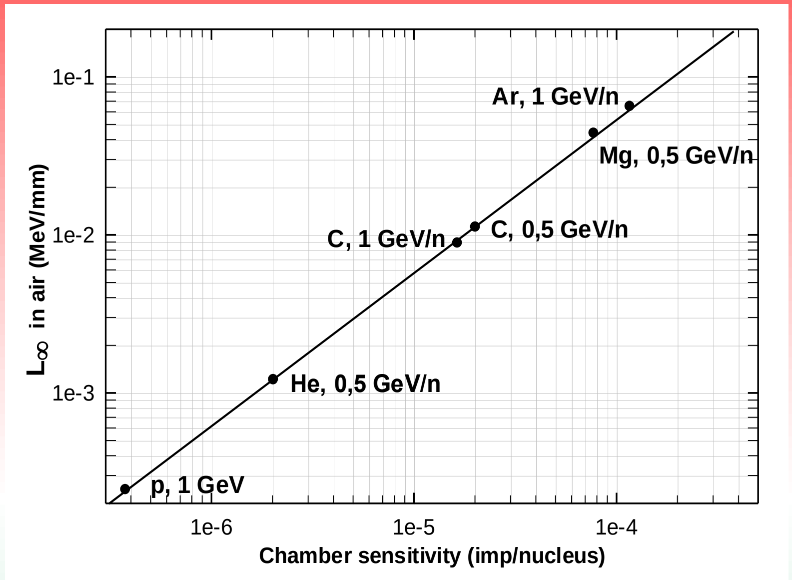

The dosimetric ionization chamber calibration at the Nuclotron beams by the activation detectors

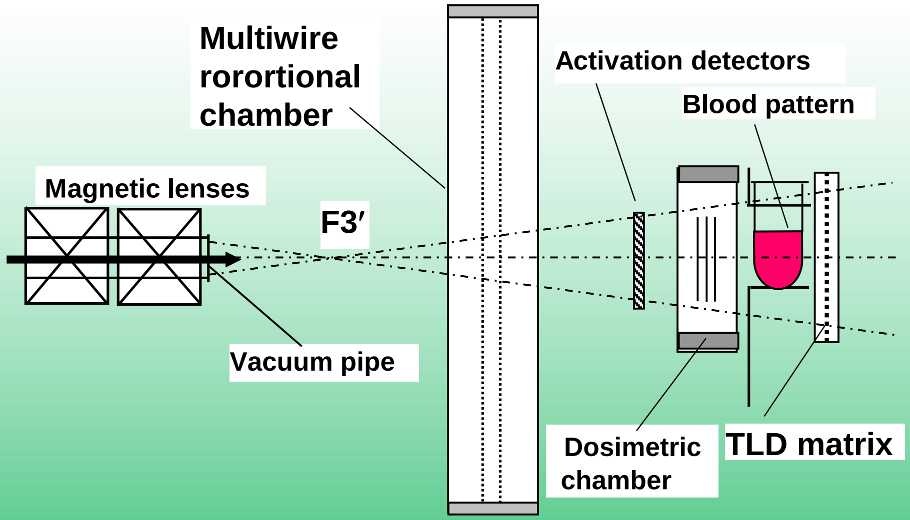

The experimental arrangement at radiobiological exposures at the Nuclotron

Nuclei	p	He	C	C	Mg	Ar	Fe
Energy GeV/n	1	0.5	1	0.5	0.5	1	1.25
LET in blood keV/μm	0.233	1.157	8.40	10.65	39.62	75.5	151.4

List of radiobiological experiments at the Nuclotron

Beam channel at Nuclotron for research in radiobiology. Well-controlled ion beam (from protons and deutrons to Carbon, Fe, Xe) with energy from 300 to 1000 MeV/u allows cell scanning and to define the degree of radiation damage.

Damages of the higher nervous activity centers

Experiments with monkeys (JINR – IMBP RAS).
Protons 170 MeV, C6+ nuclei 500 MeV/u

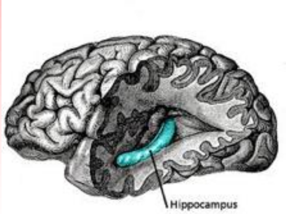

hyppocampus

Tracks of iron ions are well visualized with markers of double-strands of RNA (γH2AX)

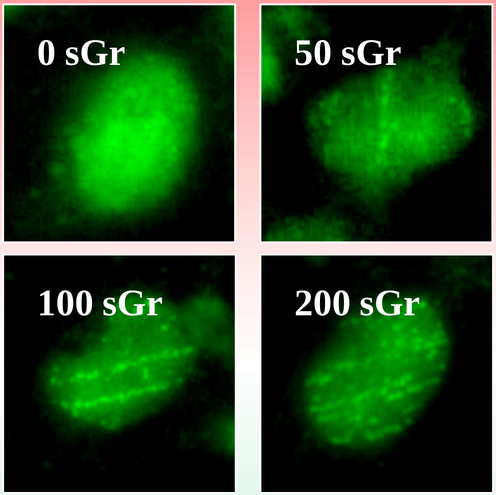

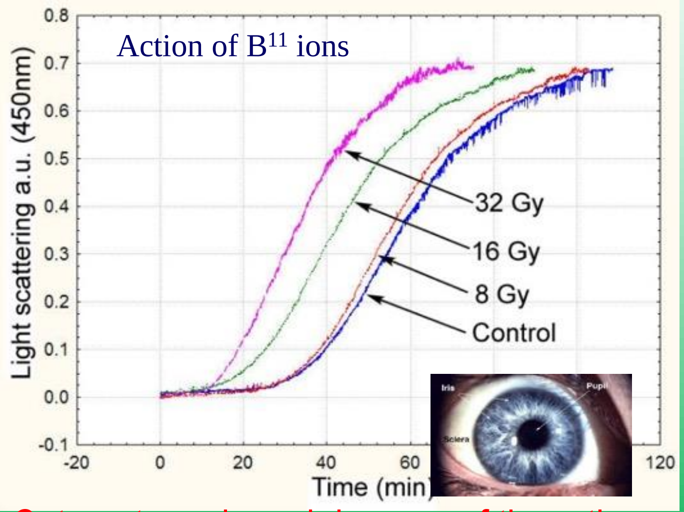

Cataractogenic and damage of the retina

Development of the prototype units Complex of Carbon Radiotherapy

The foundations of hadrontherapy

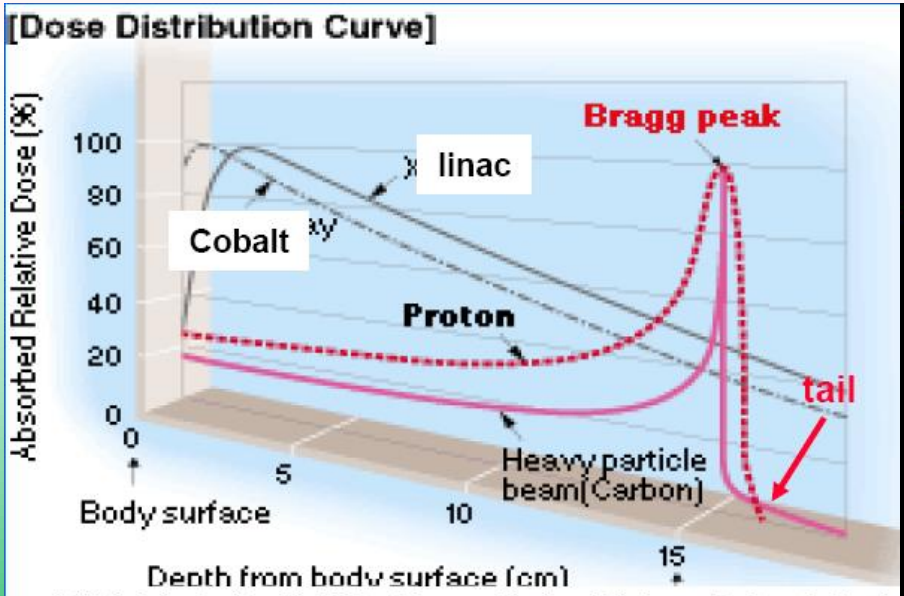

httt://global.mitsubishielectric.com/bu/particlebeam/index_b.html

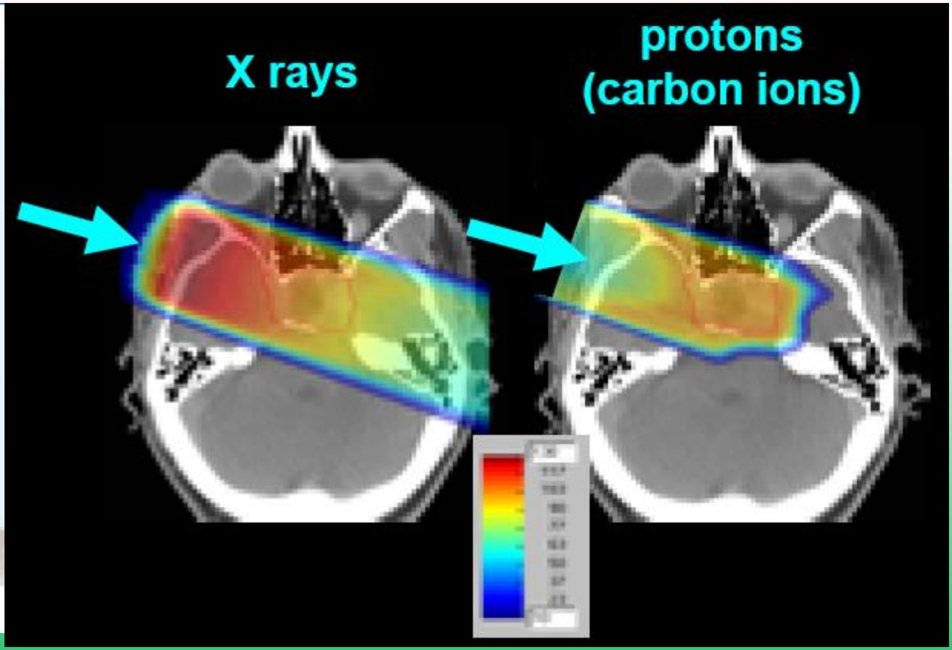

Block diagram of the experimental setup of the prototype on a carbon nuclei beam of the Nuclotron-M

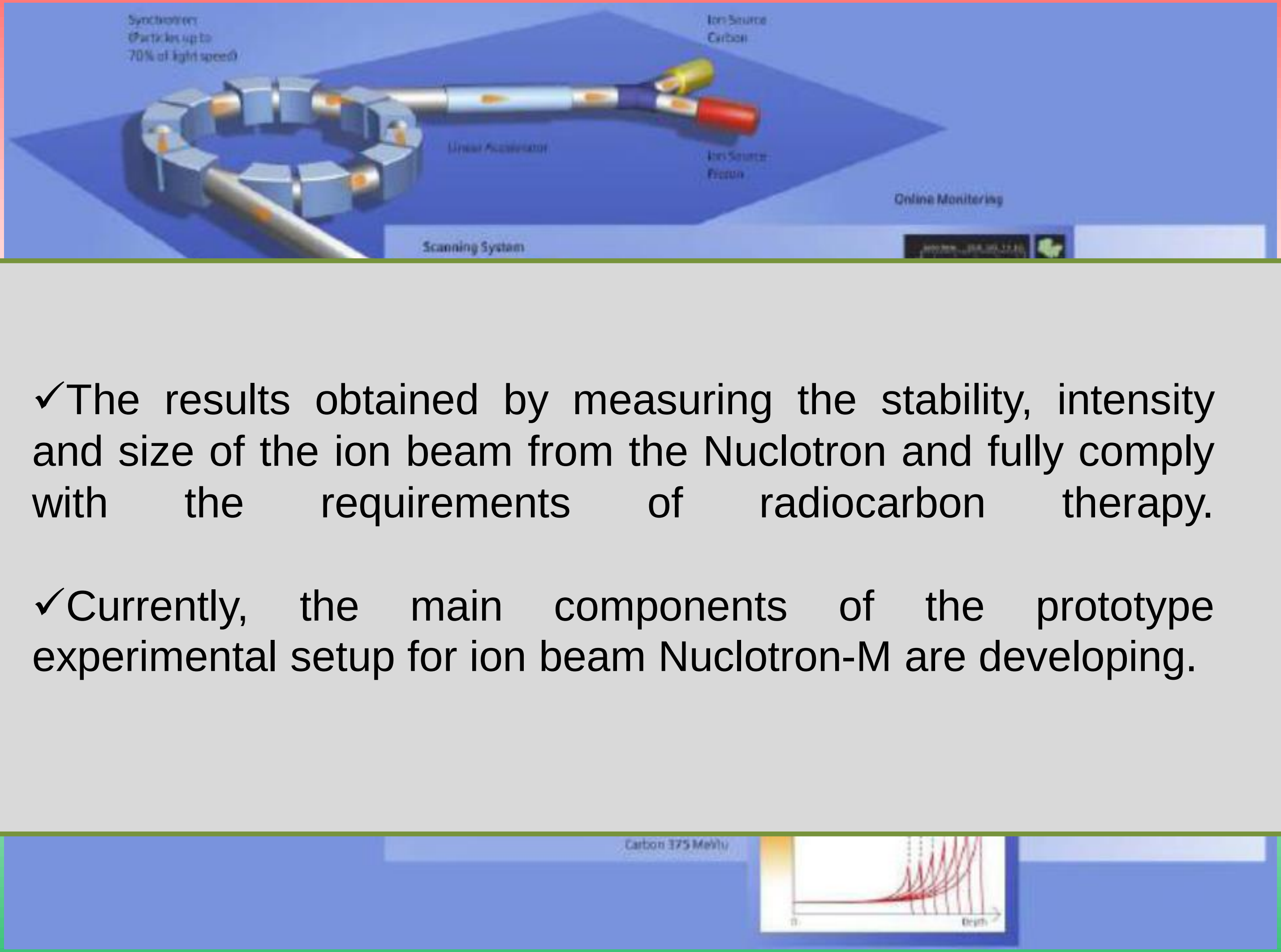

✓The results obtained by measuring the stability, intensity and size of the ion beam from the Nuclotron and fully comply with the requirements of radiocarbon therapy.

✓Currently, the main components of the prototype experimental setup for ion beam Nuclotron-M are developing.

A set of detectors and electronics for complex of Carbon therapy is shown below.

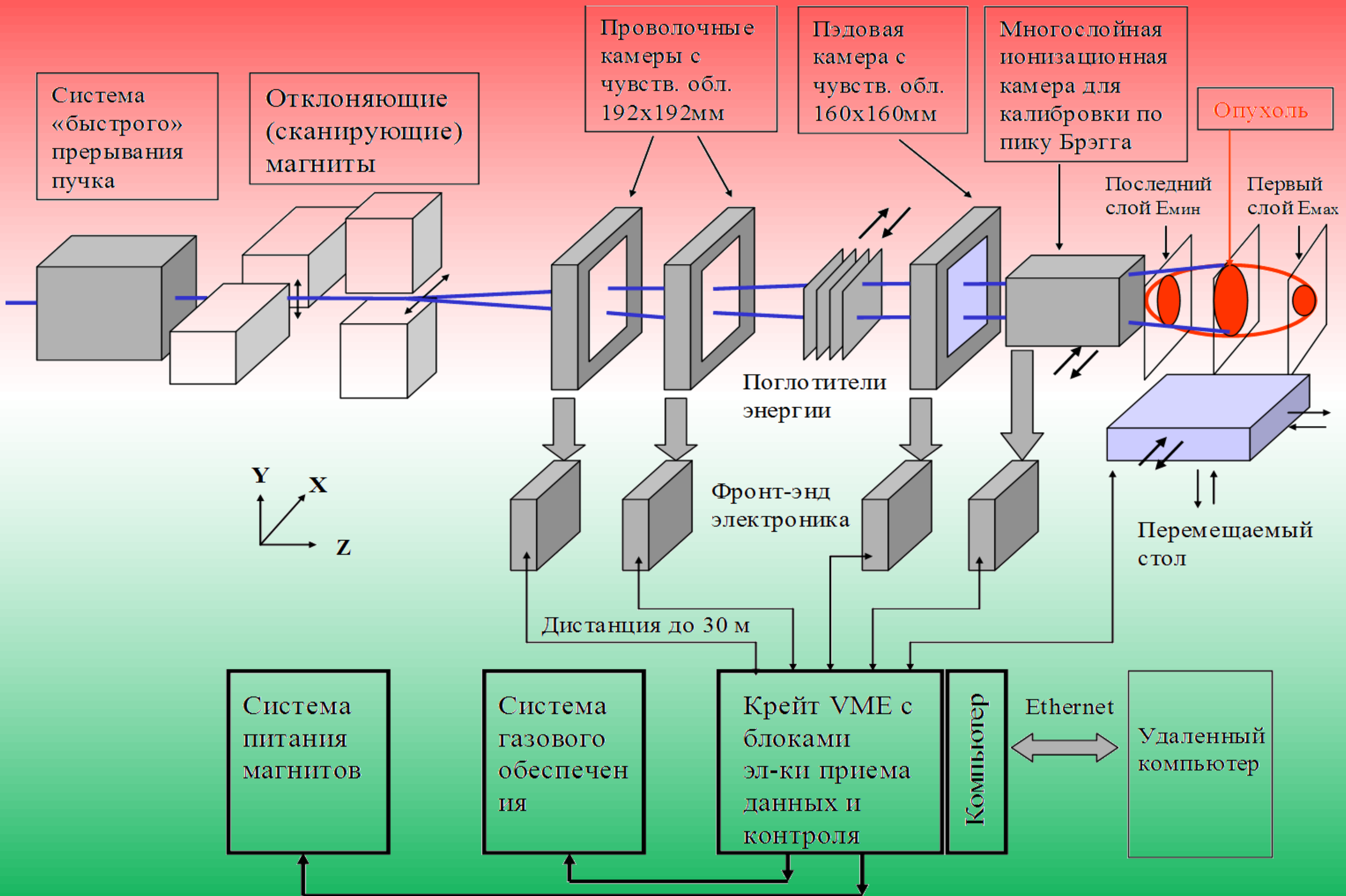

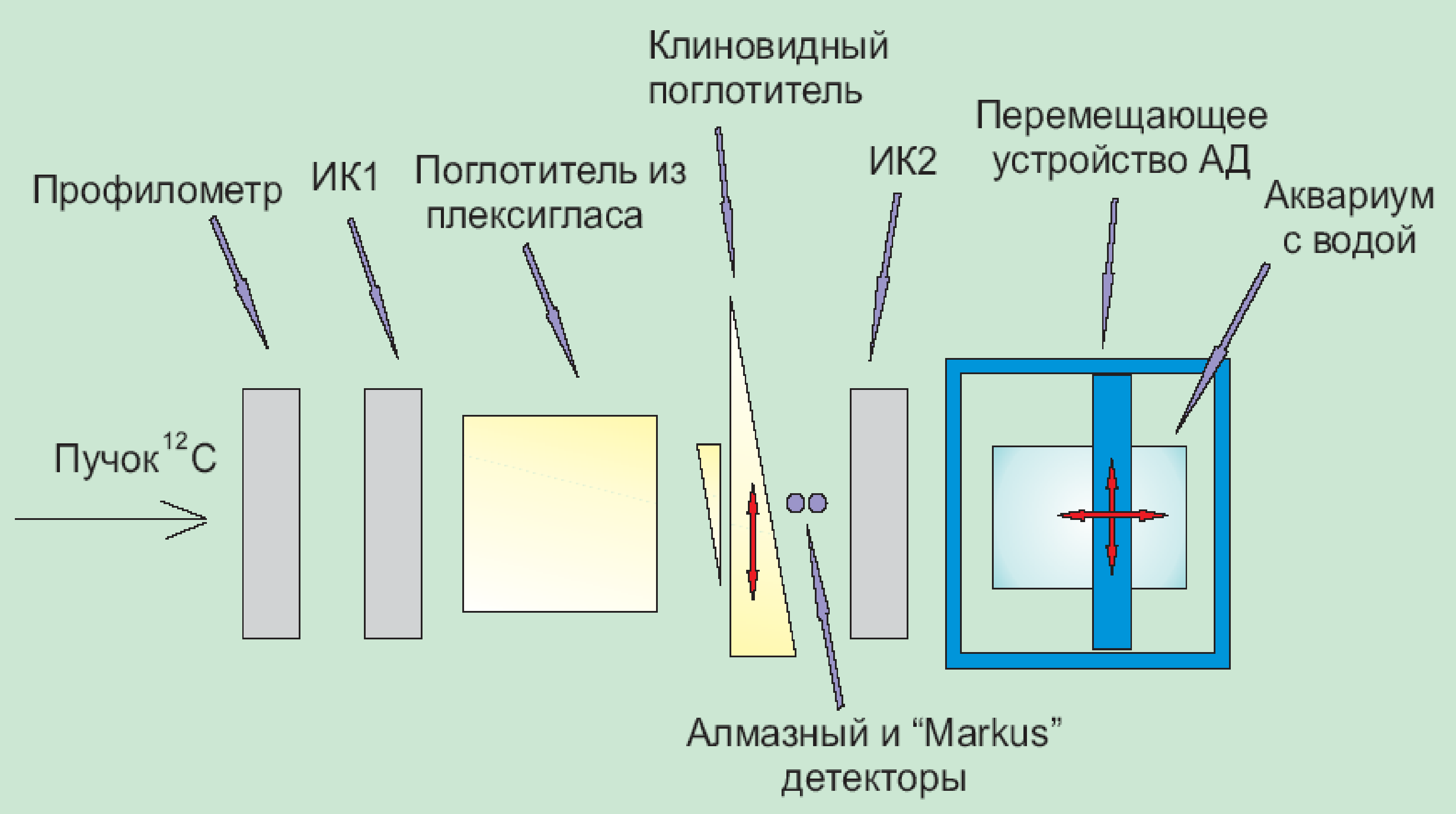

The experimental setup "Med-Nuclotron"

Profiles of the beam of accelerated ions 12C were measured using an multi wire chambers with 32 horizontal and 32 vertical wires with a 3 mm.

horizontal profile

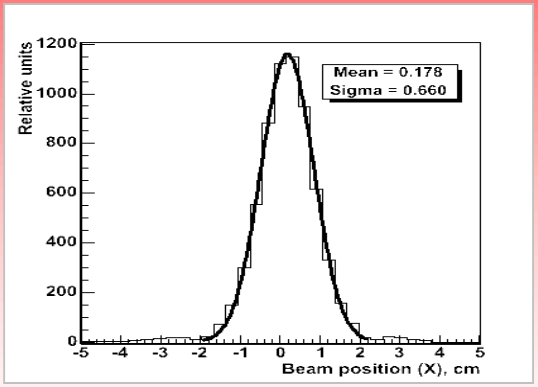

vertical profile

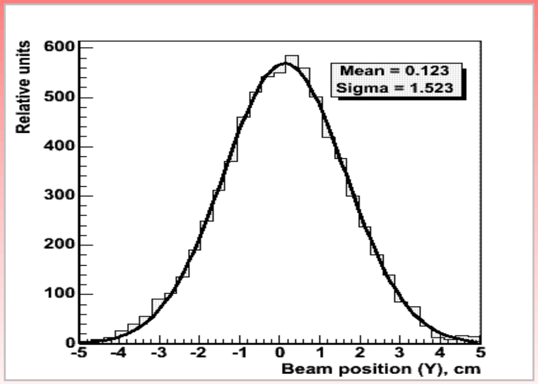

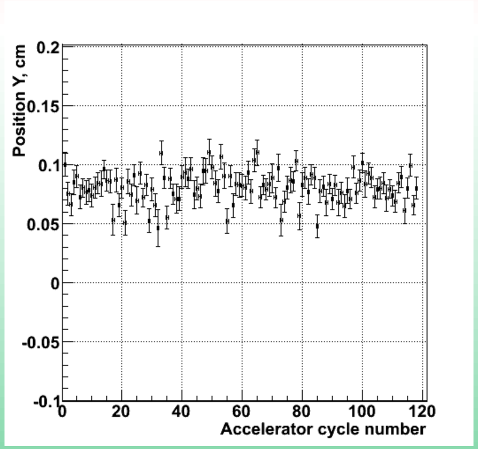

Beam position during the one irradiation run.

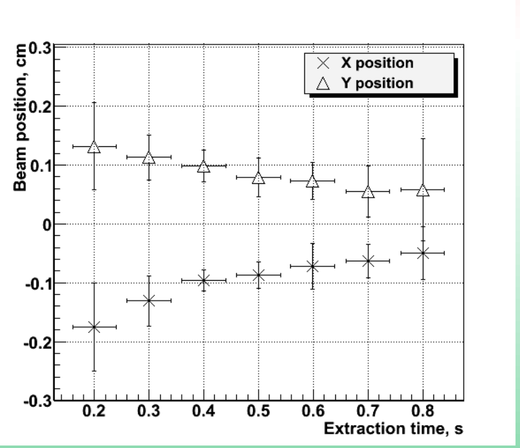

Beam position during the extraction

The beam profile of carbon ions

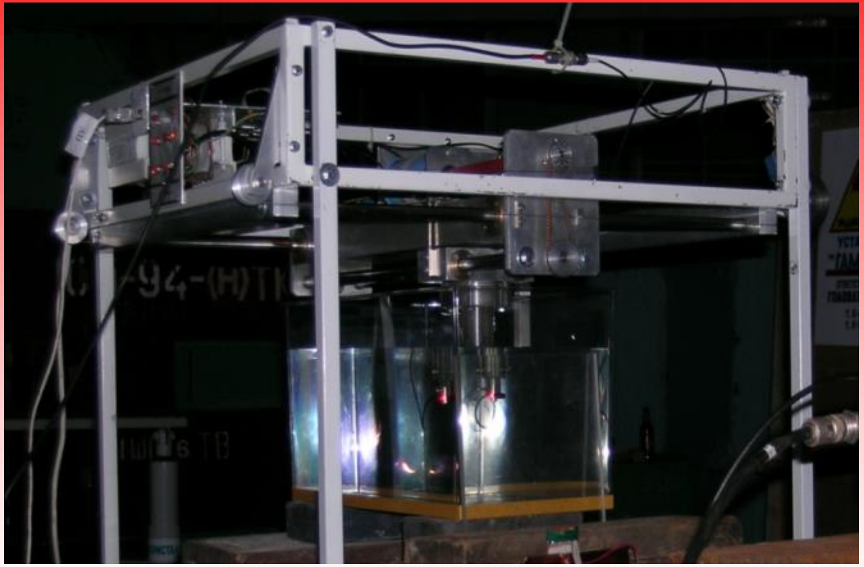

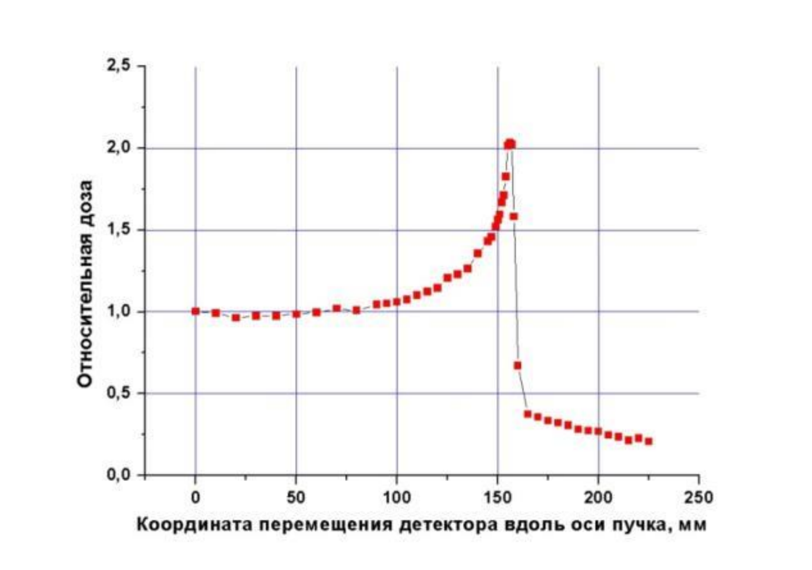

Diamond detector can be moved along and across the beam move the device with 1 mm increments. The photo shows a detector moving in the aquarium with water.

Bragg peak while moving along the beam axis diamond detector in water phantom.

Measurement of the Bragg peak in water phantom

Device structures tracks of heavy ions, filled with nanoparticles

Electrodeposition of nanoparticles

✓The method provides high selectivity (local) deposition.

✓Using the low (room) temperature in the electrochemical deposition of

A new direction in the field of nanotechnology is devoted to creation of nanostructures within a track that creates a heavy ion in the silicon wafer, and can be implemented composite structure - ferromagnetic, paramagnetic.

substances - solid solutions chalcogenides, alloys of several metals (not only the equilibrium, but also the composition of the non-equilibrium), complex oxides, the metal chalcogenide systems and others.

Extent filling of the pores with Ni nanoparticles is controlled by deposition time

On the basis of silicon created a structure with magnetic nanoclusters Ni.

Giant magnetic resistance n-Si / SiO2 / Ni nanostructures

Fedotov A., Ivanou D., Ivanova Yu., Mazanik A., Svito I., Streltsov E.,
1 Belarusian State University, Independence av. 4, 220030 Minsk, Belarus
Tyutyunnikov S.
2 Joint Institute for Nuclear Research, Dubna, Russia

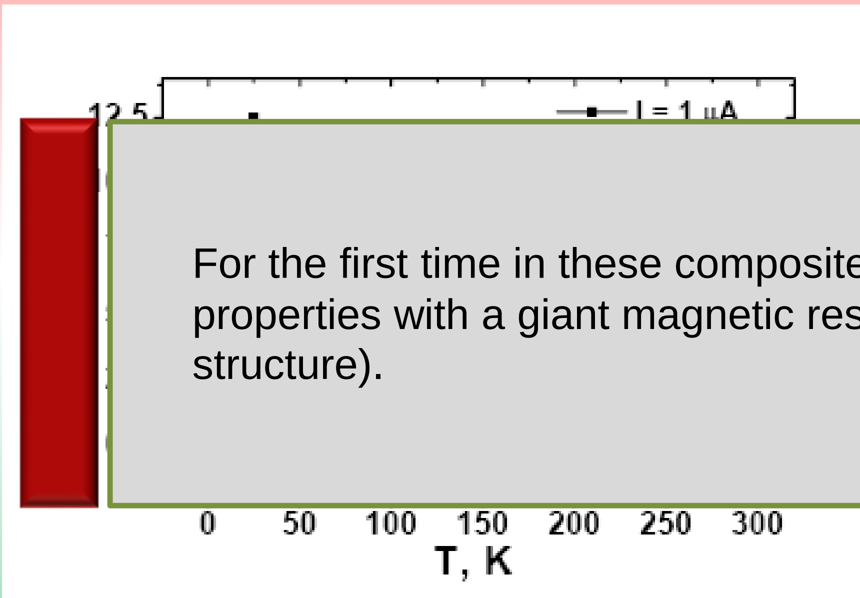

For the first time in these composite structures are obtained the material properties with a giant magnetic resistance (a prototype spintronic structure).

The dependence of giant magnetic resistance on temperature

Experimental infrastructure at the VBLHEP of JINR for research in the field of radiation material science and radiobiology

Kurchatov synchrotron radiation source

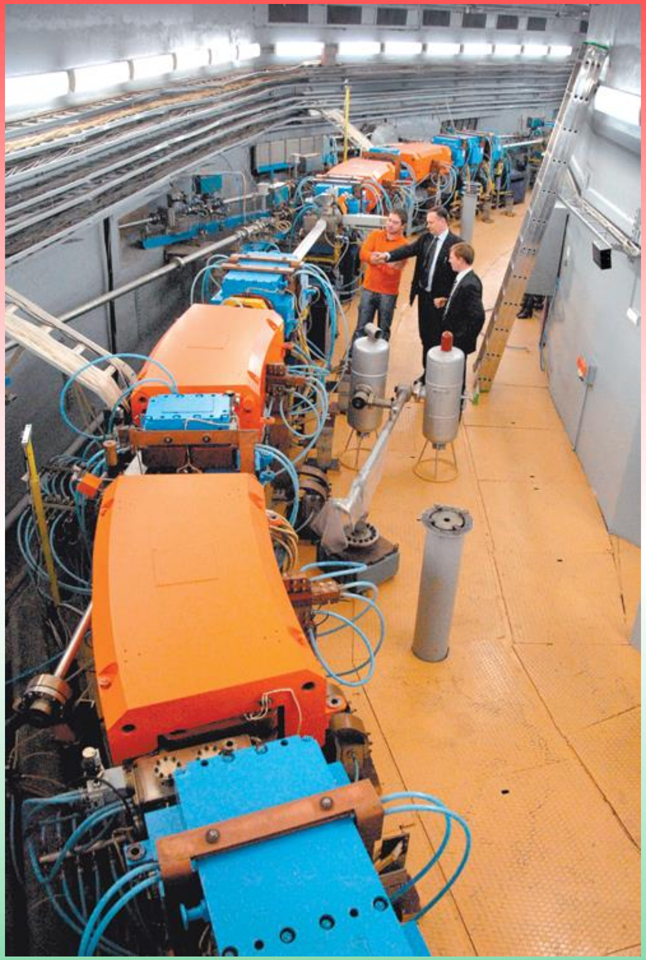

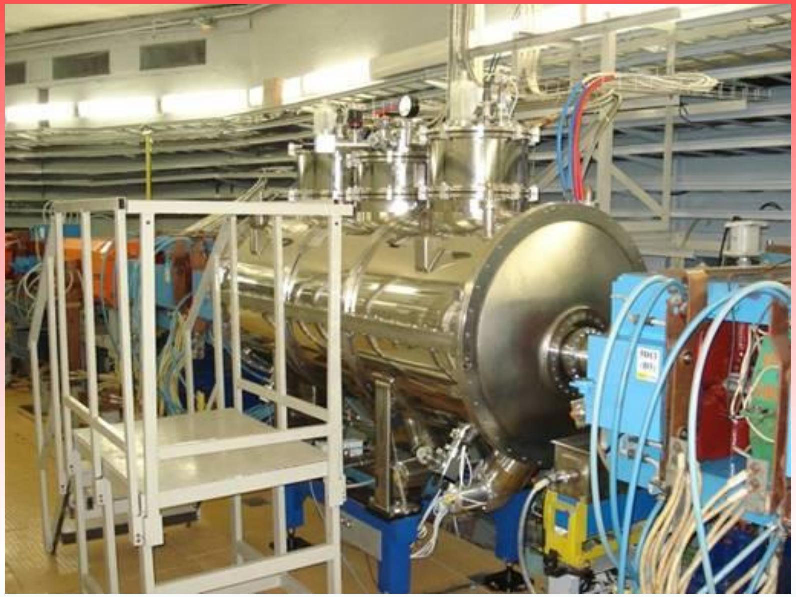

Kurchatov synchrotron radiation source (different installation)

SYNCHROTRON RADIATION

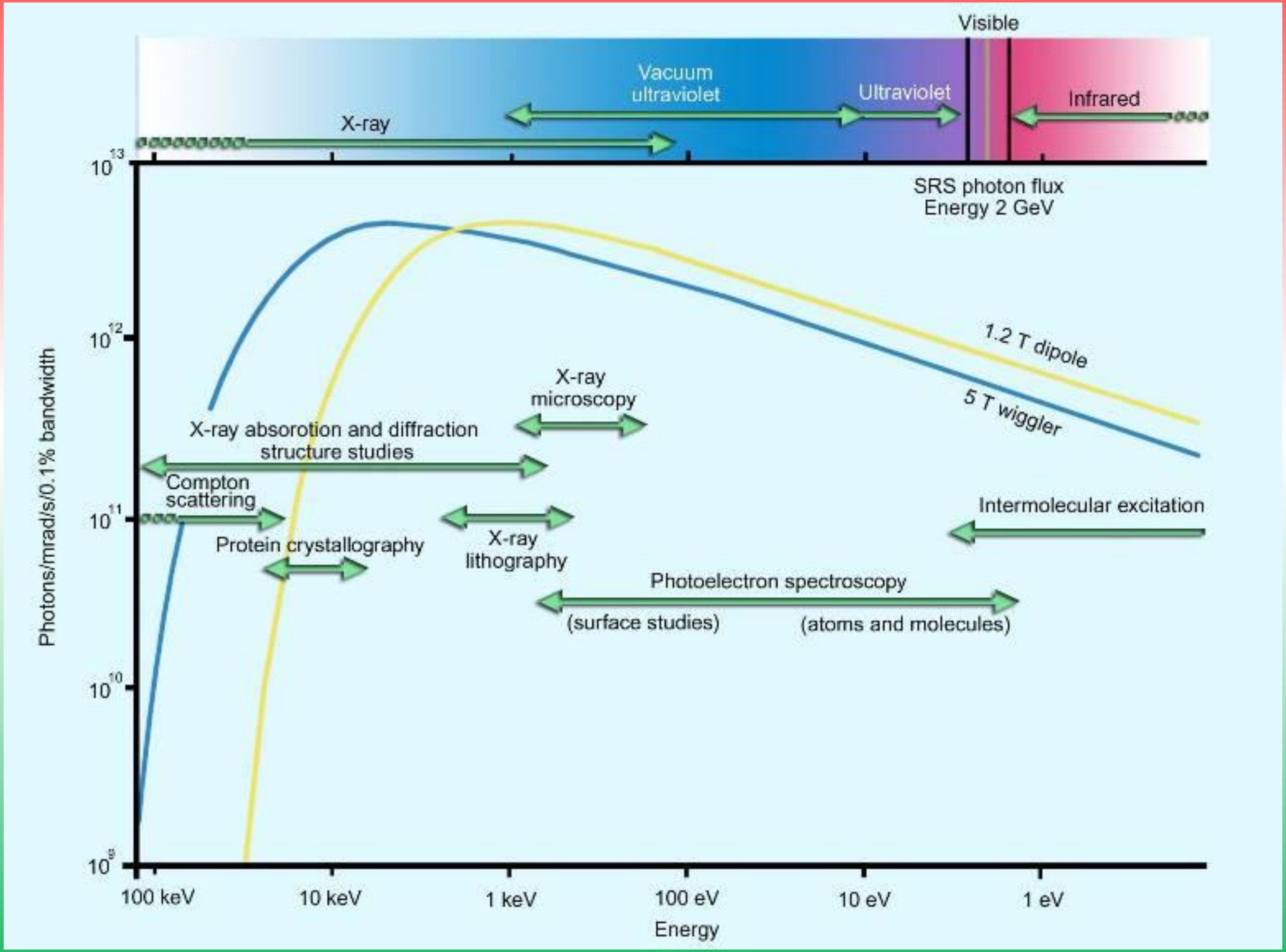

Basic scientific directions

- **Nanodiagnostics and Materials** (atomic structure, macromolecular structures, nanofilms, heterostructures, superlattices, nanoclusters, fine (fine dispersed) environment, quantum dots, radiation defects, carbon nanostructures and nanocomposites, etc.).
- **Nanotechnology** (molecular-beam epitaxy, a technique Langmuir-Blodgett films, etc.).
- **Biotechnology** (protein crystallography, organic film on the surface of the liquid, etc.).
- **Microsystems** technology (LIGA - technology)
- **Fundamental research** (materials at ultrahigh pressures, "space" crystals, X-ray optics, etc.).
- **Living systems and nuclear medicine** (new methods of medical diagnostics, supramolecular structure of biological tissues and fluids, etc.).
- **Dual-use technologies** (non-destructive testing responsible products, forensics, etc.).
- **Metrological support of nanotechnology** (Spectroradiometry, metrology layered structures, etc.).

Development of EXAFS spectroscopy methods on SR beams

The main scientific problems which can be solved by using ED EXAFS

1. The investigations of state matter in extreme condition $P \leq 40$ GPa, $T = 2000 \div 3000\ ^0C$
2. The investigation of kinetics passing chemical reactions in heterogeneous systems with time resolution $\leq 10^{-3}$ sec
3. The investigation of magnetic properties of nanostructure composite films with using magnetic dichroism
4. The structure investigation with femtometer resolution
5. The investigation of phase transition under external actions (magnetic and electric field, radiation).

The basic units of the station "Energy dispersive EXAFS spectrometer"

General view of the spectrometer inside the hutch.

XASX-Ray Absorption Spectroscopy

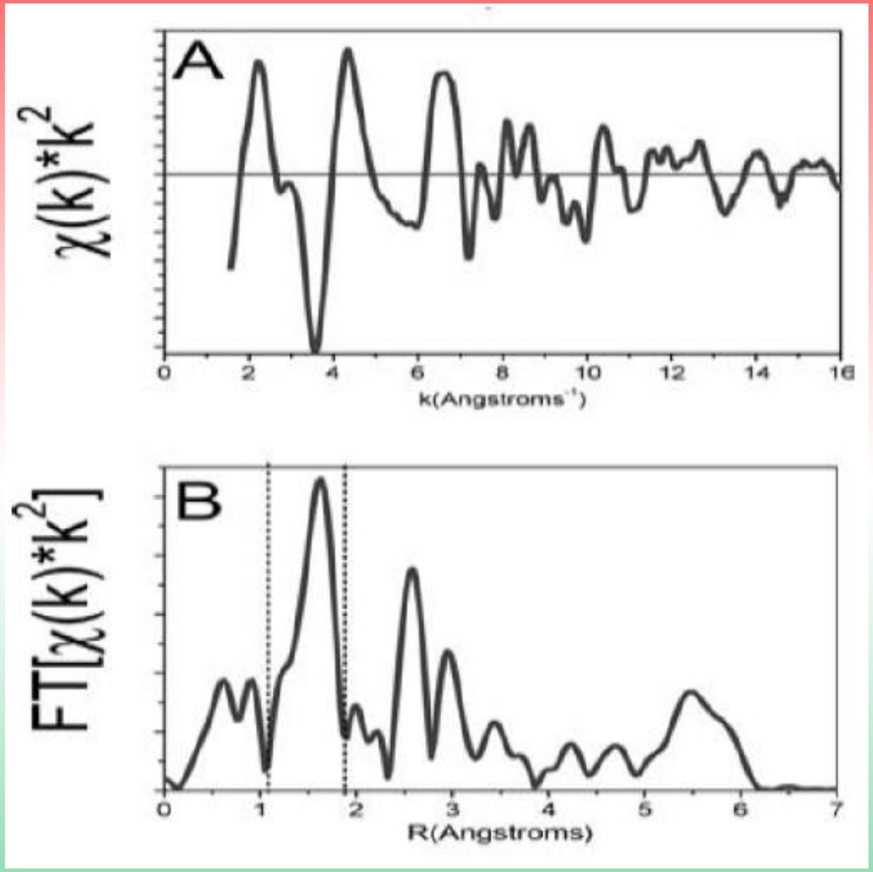

$$k = \frac{\left[2m(E - E_0)\right]^{1/2}}{\hbar}$$

$$\chi(k) = \frac{\mu(k) - \mu_0(k)}{\mu_0(k)}$$

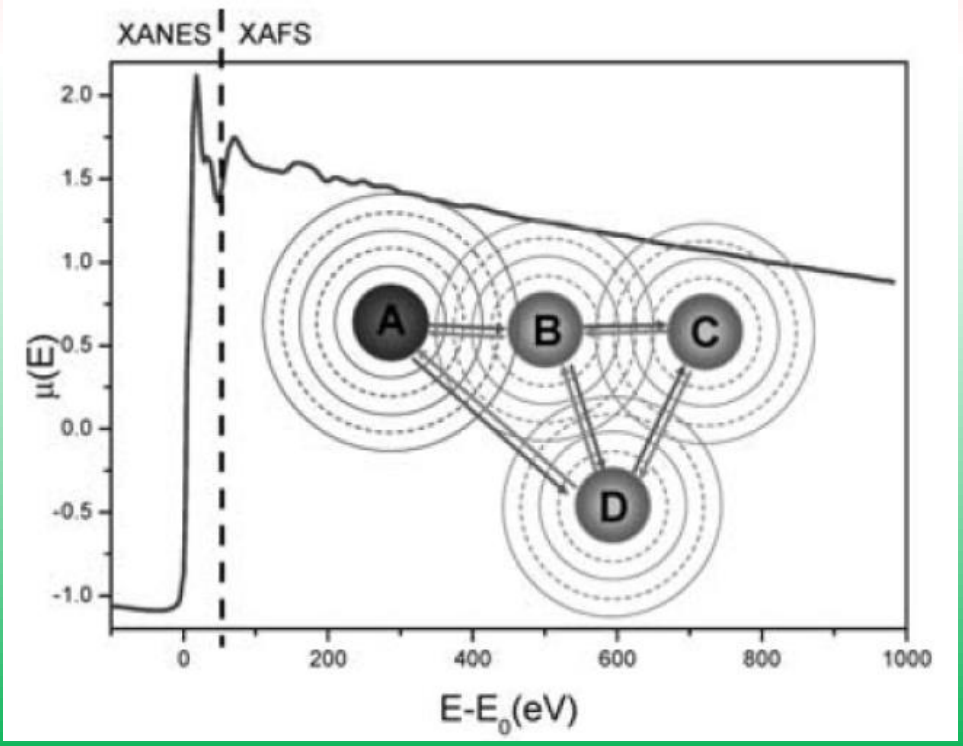

Fourier transform of the EXAFS spectra *at the CoK-edge for the $La_1xSrxCoO_3$*

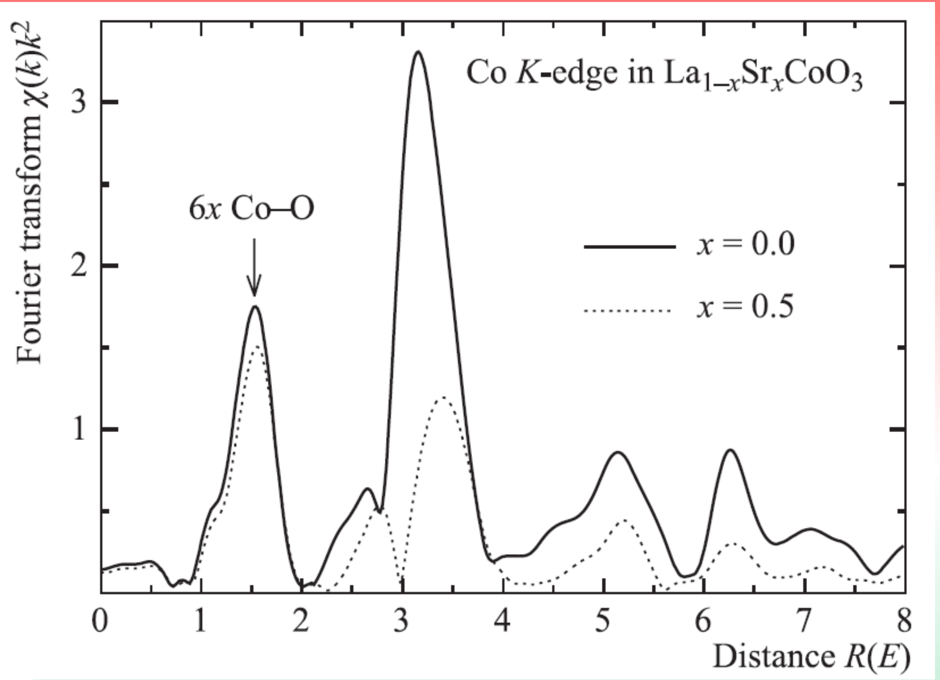

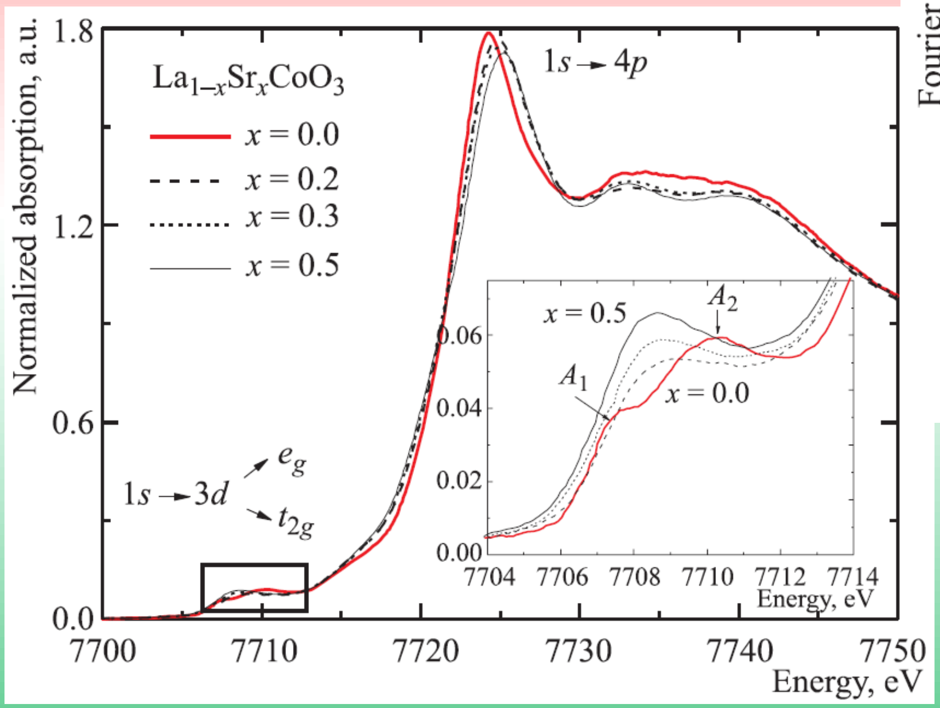

XANES spectra at the Co *K-edge for the $La_1xSrxCoO_3$ (x0.00.5). Inset: the pre-edge region*

Debye-Scherrer diffraction geometry "reverse" on the scattering of the Kurchatov source SI

Debye-Scherrer diffraction with registration in the opposite hemisphere

The advantages

1. Very high sensitivity to the relative change in the interplanar distances - two - three orders of magnitude higher than the scattering of the "forward"

Disadvantages

1. Investigated only a thin surface layer – hundreds Microns.
2. The sample must be flat and smooth (for maximum sensitivity)
3. In the study on line stretching occurs along one axis, and the measurement - at a different (Poisson's ratio)

Diffraction in the opposite hemisphere based on equipment of EXAFS – D spectrometer

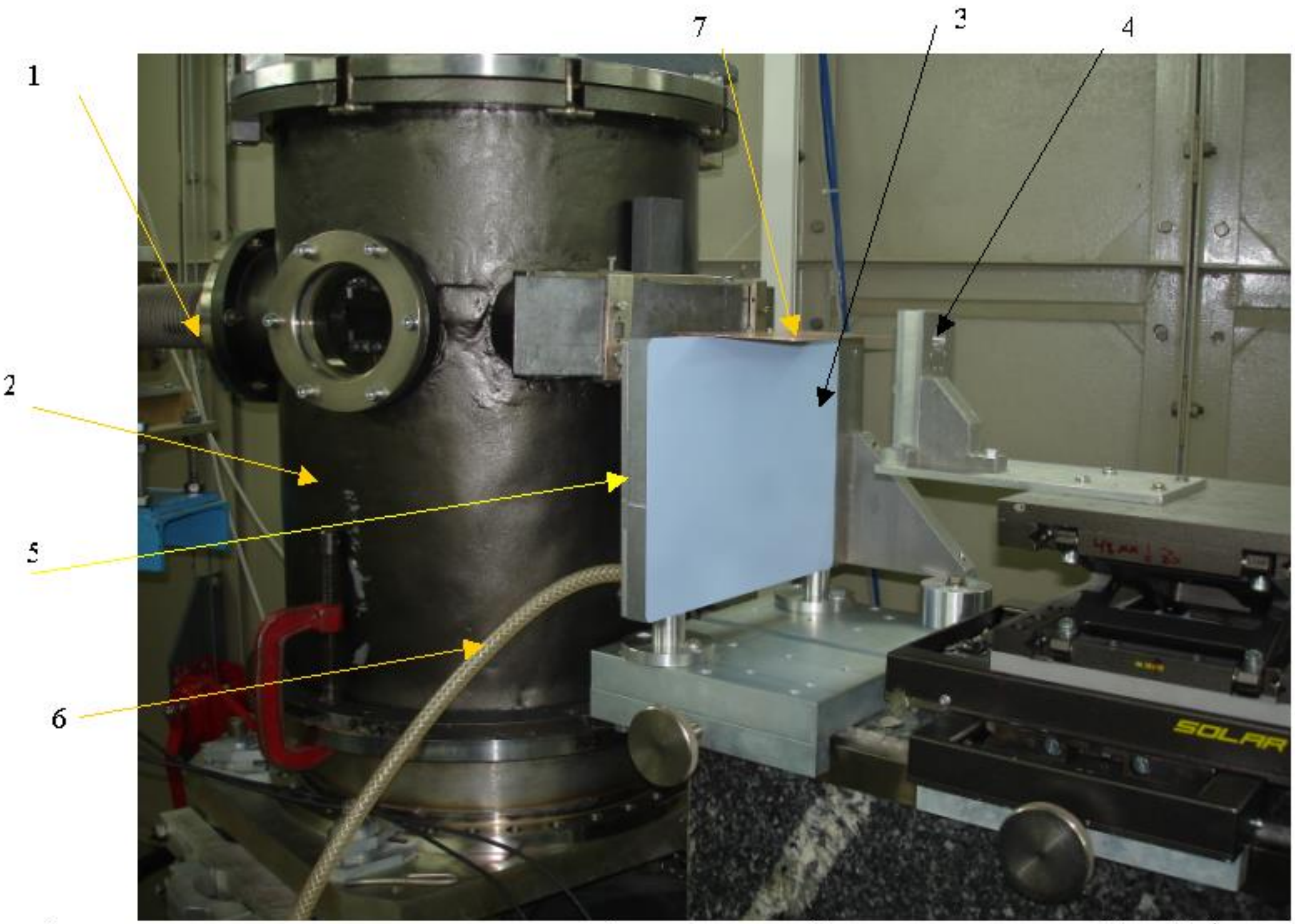

Экспериментальная станция для прецизионной регистрации дифрактограмм по методу Гуля/Дебая-Шерера в геометрии обратного рассеяния. 1- канал вывода СИ, 2 - вакуумно-гелиевый колпак монохроматора, 3. 2D детектор, 4 – кронштейн исследуемого образца, 5 – кронштейн-«присоска» регистрирующего экрана, 6 - шланг откачки «присоски» регистрирующего экрана, 7 - экран рассеянного на воздухе излучения.

Debye-Scherrer diffraction in the opposite hemisphere

The interplanar distance of the heat-treated sample is less than control. d/d =$5.7*10^{-4}$

Profile ring heat-treated sample is wider than control ring in 3.6 times.

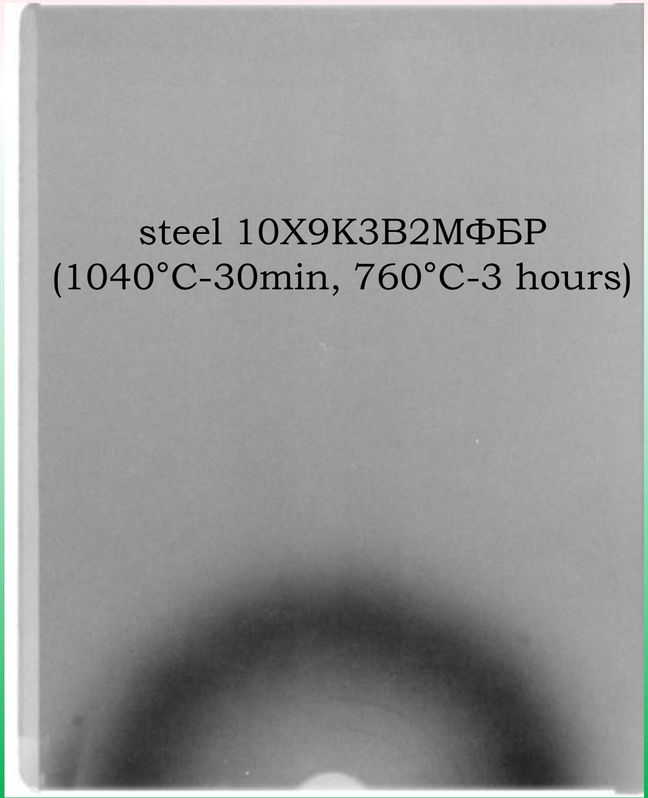

Debye-Scherrer diffraction in the forward hemisphere. Corundum. (Reference Model)
Experiment.

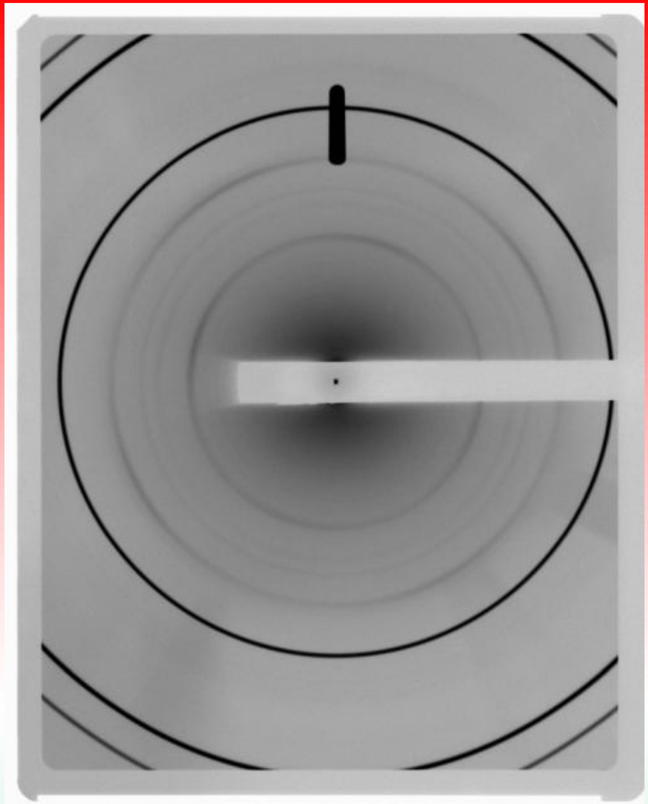

Debye-Scherrer diffraction in the backward hemisphere. Steel body of Balakovo NPP. Experiment.

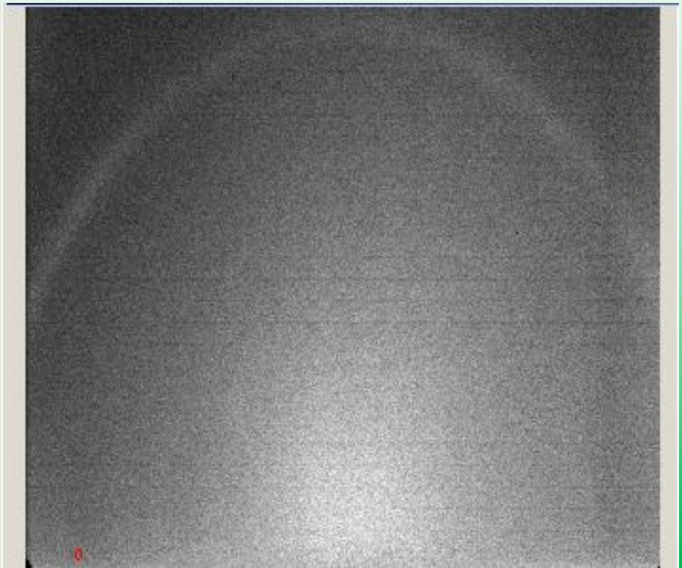

Raman scattering is the interaction of photons and intrinsic molecular bonds

Raman Chandrasekhara Venkata

7.11.1888, Tiruchchirappalli, — 21.11.1970, Bengaluru

The Indian physicist, awarded the Nobel Prize on the physicist 1930 for opening of combinational dispersion of light (Raman effect).

Molecular vibration in sample

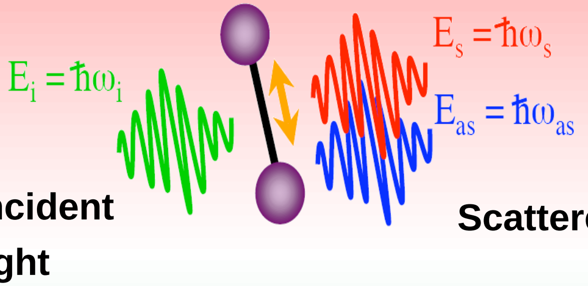

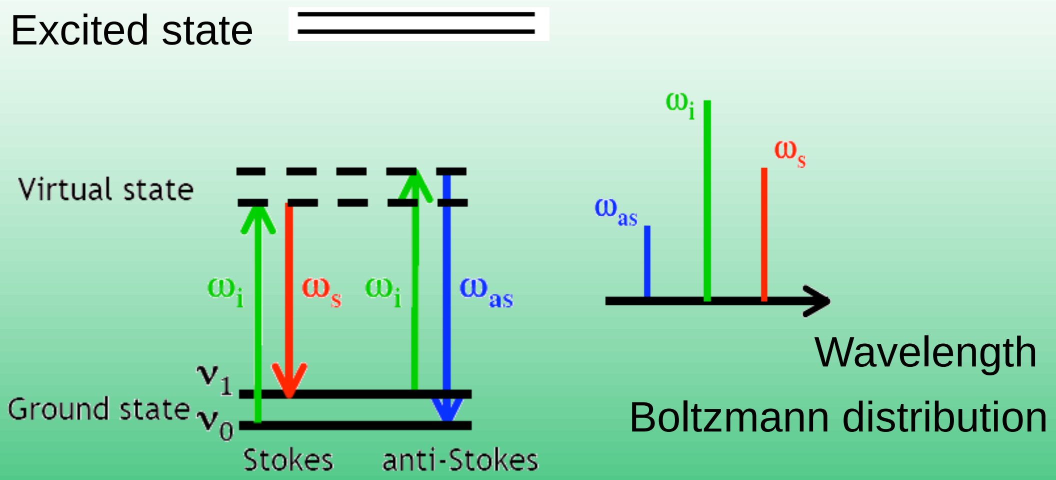

Raman and CARS-microscopy.

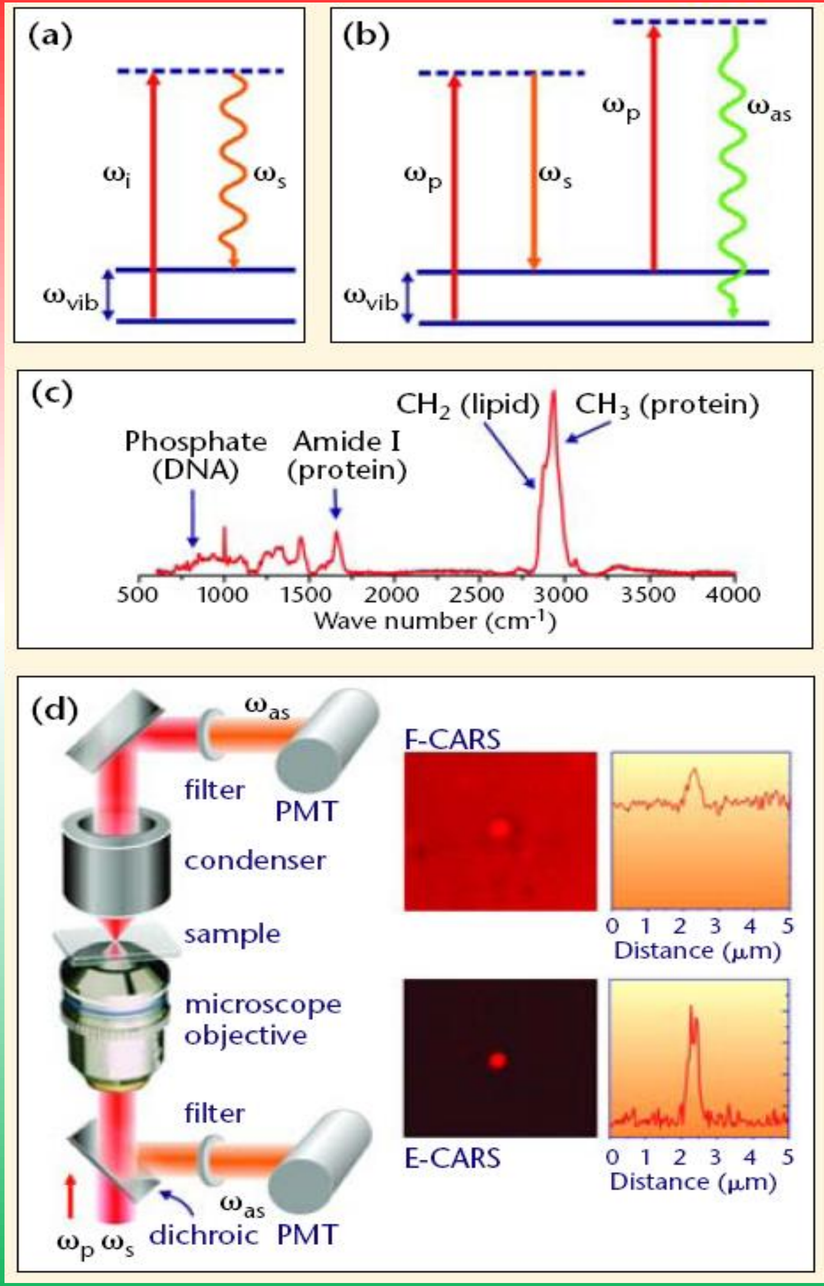

(a) Spontaneous Raman energy diagram based on inelastic scattering of incident radiation resulting in a red-shifted (ω_s, Stokes) emission.

(b) CARS energy diagram in which the vibrational oscillators are actively driven at ω_p-ω_s. Upon further interaction, a blue-shifted (ω_{as}, anti-Stokes) photon is emitted.

(c) Raman spectrum of dried HeLa cells showing the wealth of molecular information contained in the vibrational spectrum.

(d) Basic layout of CARS microscope with a collinear excitation geometry. Either the sample or the beams are scanned.

Signal is detected simul-taneously in the forward (F-CARS)and the backward (E-CARS) direction, yielding different contrast mechanisms.
F-CARS signals are strong and are accompanied by a nonresonant background from the medium while E-CARS signals are weak and the background is sup-pressed.
This is illustrated by the images of a 0.2 μm polystyrene bead in agarose taken at the 3,050 cm^{-1} aromatic CH vibration of polystyrene.

Scanning Confocal Microscope

- ***Sub-μm spot Scanning Spectroscopic Microscope***
- ***Laser Confocal Microscope***

3-D tomography by confocal laser microscope based on cross-section spectroscopy at 0.2 μm spot

Raman, fluorescence and lifetime analysis of compounds, contaminants; defects and stress in semiconductor;

films, liquid crystal, biological saline…

Basis of the piezospectroscopic effect

the applied stress strains the lattice and alters the energy of transitions between electronic states

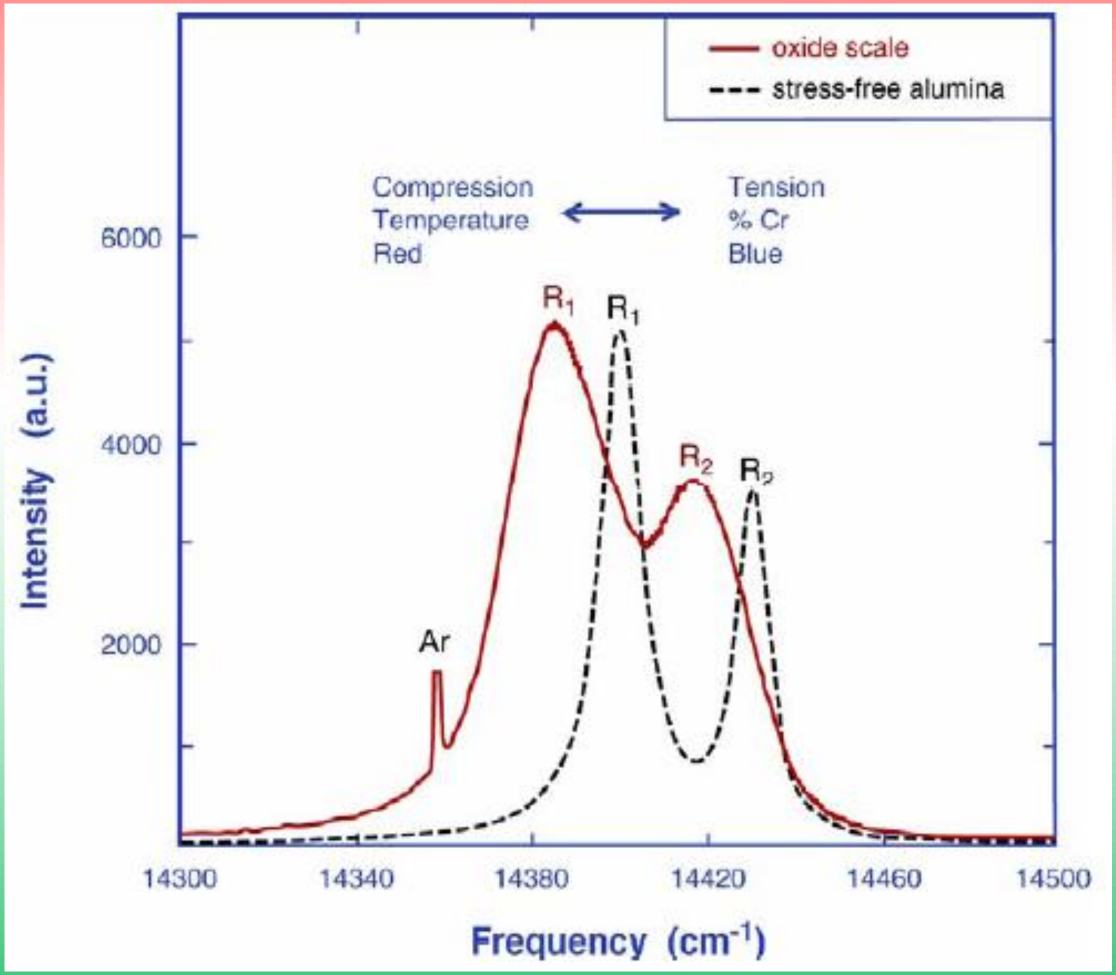

R-lines shift :

$$\Delta\nu = \Pi_{ij} \times \sigma_{ij}$$

Π_{ij} – piezospectroscopic coefficients

For hydrostatic stresses:

$$\sigma_h \text{ (GPa)} \approx \Delta\nu_2(\text{cm}^{-1}) / 7.61$$

For nonhydrostatic stresses:

$$\sigma_{11} = (\Delta\nu_2 - 2{,}16\sigma_{33}) / 5{,}46$$

$$\sigma_{22} = \sigma_{33} = (\Delta\nu_2 - 0{,}83\Delta\nu_1) / 0{,}88$$

D. Clarke et. al. Non-Contact Methods of Measuring Stresses in High Temperature Materials

Depth-resolved R-lines spectra on Al_2O_3Cr virgin and irradiated by 250 MeV Kr ions. Ion flux $\Phi=1\times10^{14}$ cm^{-2}

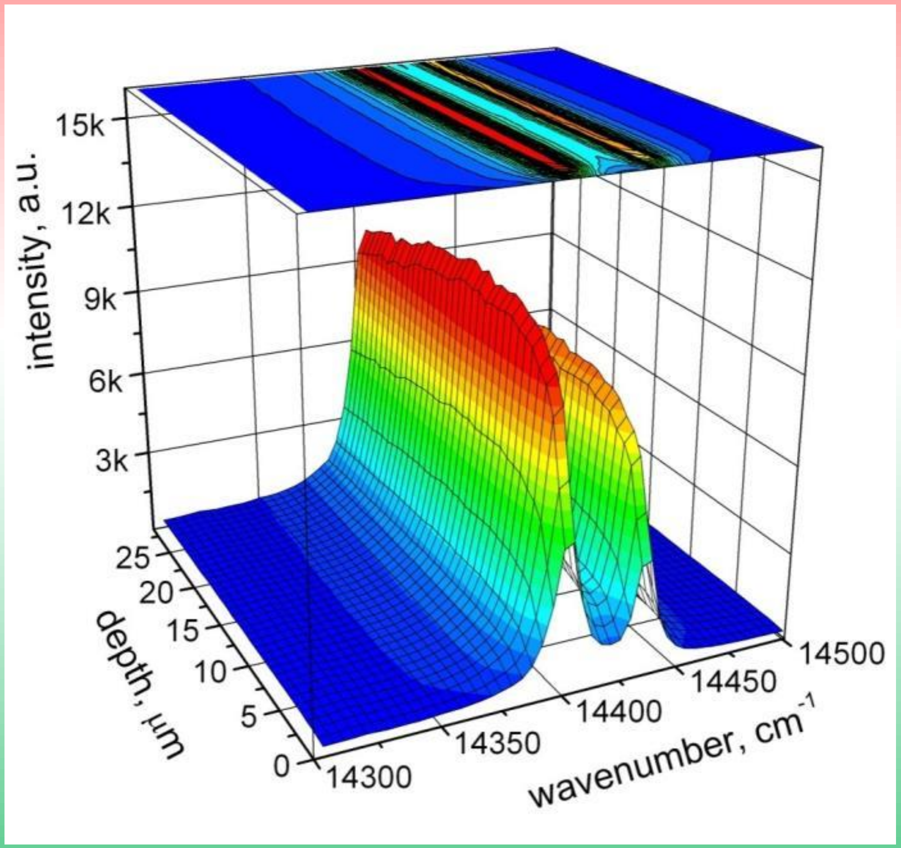

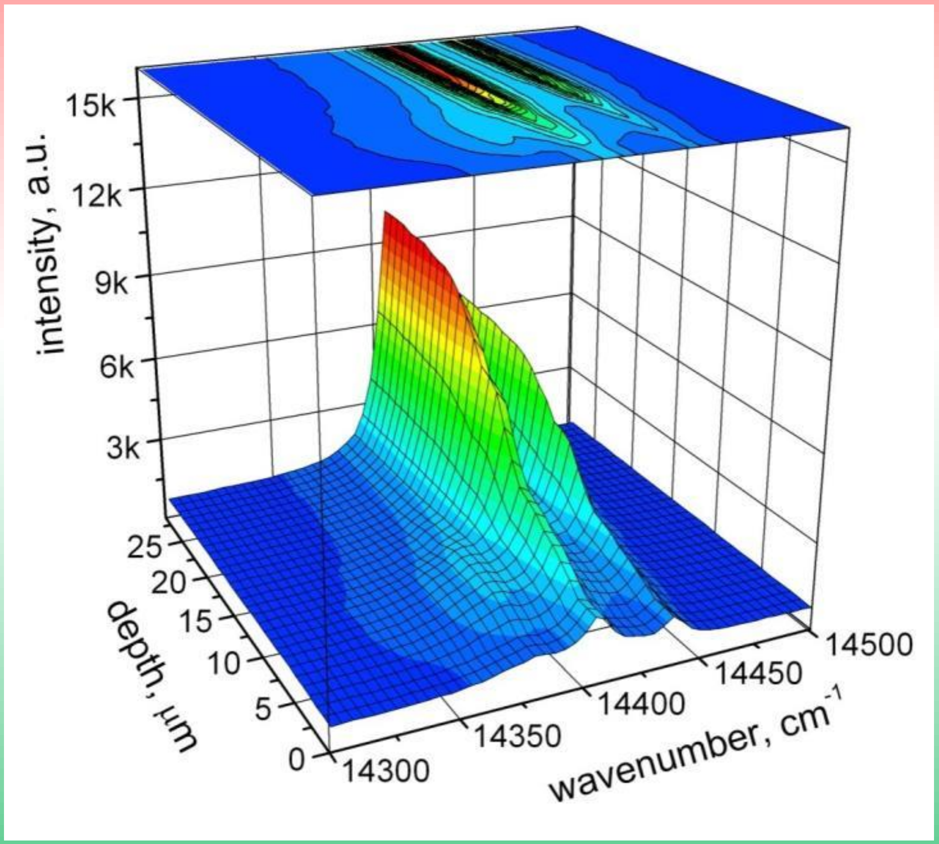

R_p=12.2 μm

Tests of nonlinear laser microscope (CARS) in Minsk before being sent to the JINR, December 2009

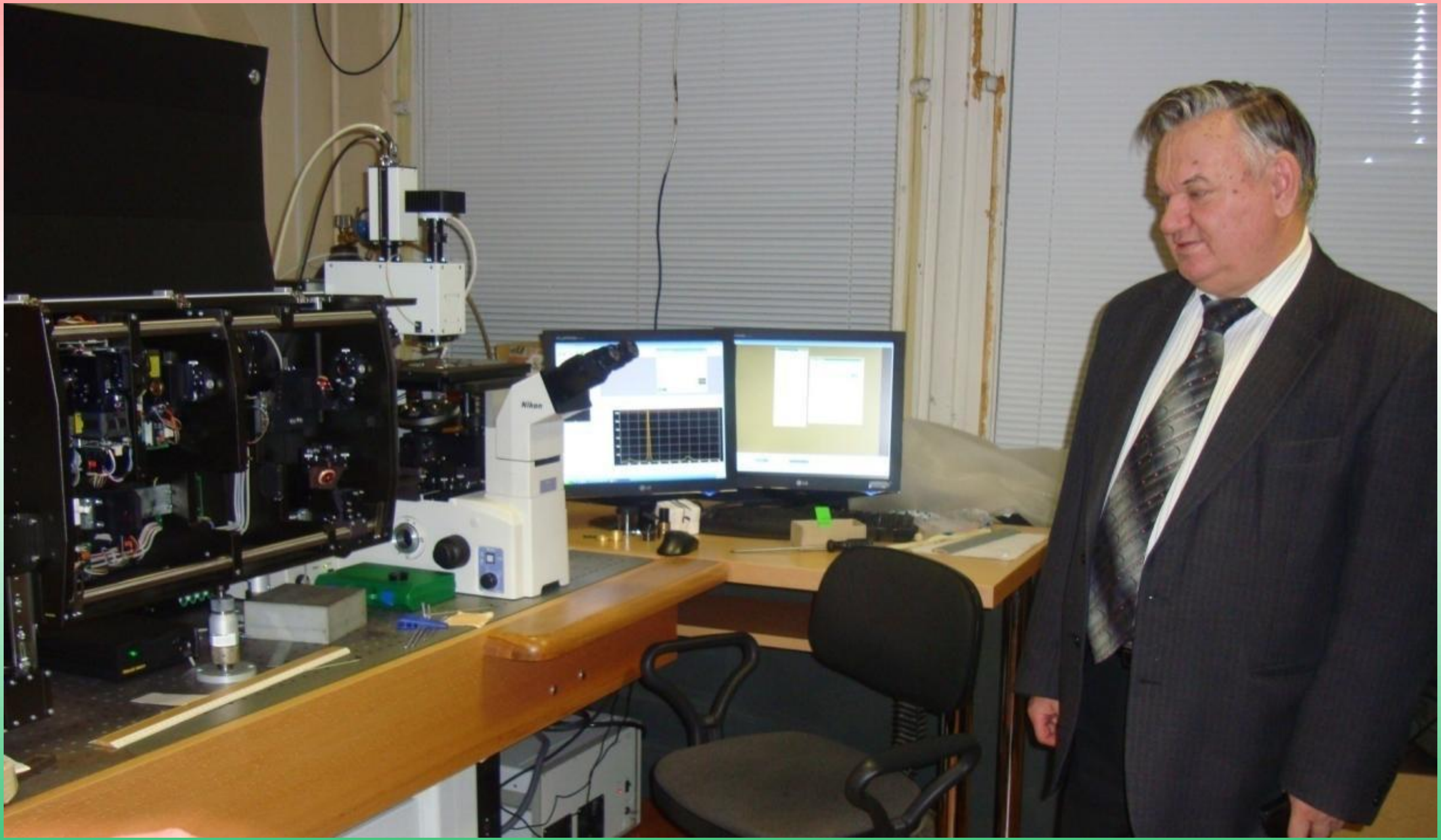

Study of apoptosis in cells with CARS microscope

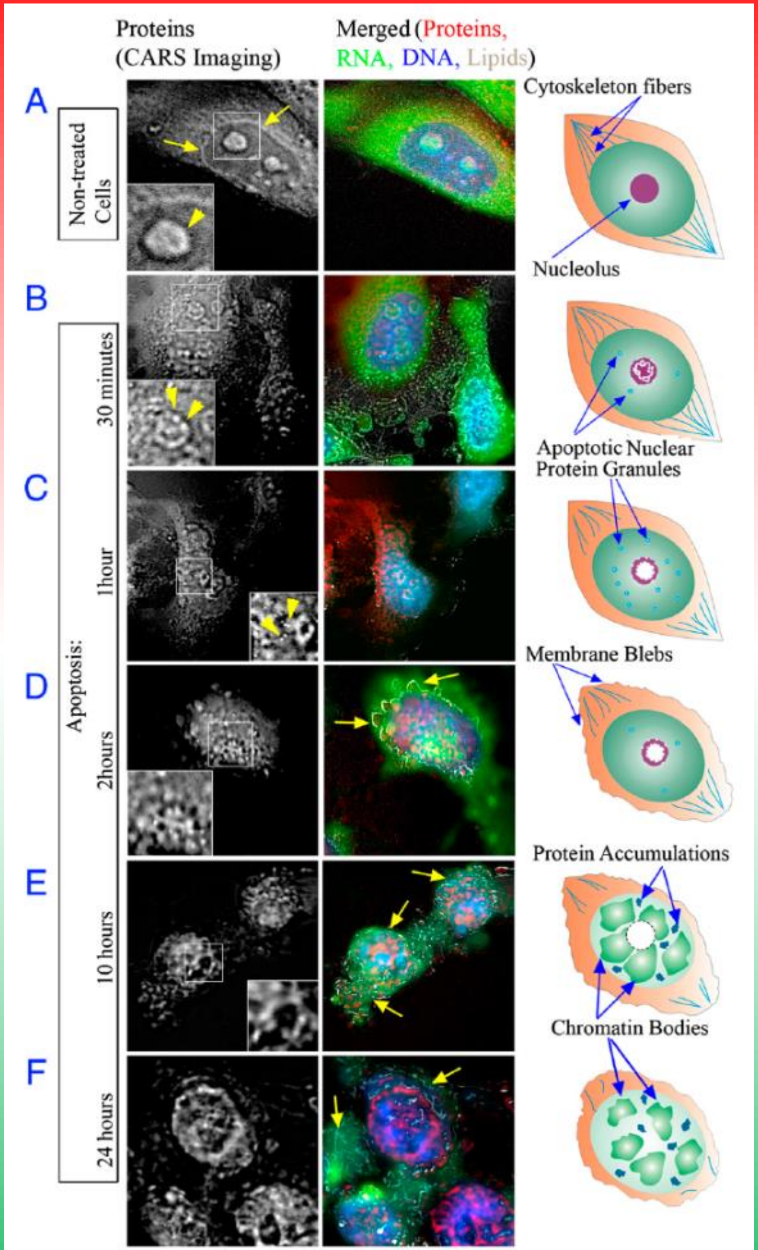

The distribution of proteins, lipids, DNA, and RNA in dividing and apoptotic HeLa cells visualized by multimodal CARS/TPEF imaging. During the imaging live cells were maintained at the physiological conditions.

Proteins and lipids were observed in the CARS mode at their characteristic vibrations of 2930 cm−1 and 2840 cm−1, respectively. Nucleic acids, stained by acridine orange, were acquired in the red (RNA) and green (DNA) fluorescence channels in TPEF mode. In the right panels, schematics of the macromolecular organization of cells are represented. The CARS signal from proteins is represented in the left panels. The panels in the middle represent merger signals of the proteins (red), RNA (green), DNA (blue), and lipids (gray). The white-outlined areas in the protein channel are enlarged below. (A) Nontreated cells. The signal from proteins is accumulated in the nucleolus (Inset, arrowhead) and the nuclear lamina (arrows). In the rest of the nuclear volume, the intensity of the protein signal is nearly uniform. (B–F) Representative cells at the subsequent stages of the apoptotic development. (B) 30 minutes following the initiation of apoptosis, the distribution of proteins is altered in the nucleolus (Inset, arrowheads) and the novel structure, apoptotic nuclear protein granules (ANPG), emerged in the nucleoplasm. In the cytoplasm, cytoskeleton fibers begin to lose their structural polarization. (C) The pattern of proteins becomes increasingly irregular, and ANPG become prominent (Inset, arrowheads). (D) The nucleolar proteins are forming a complex meshwork (Inset). The apoptotic membrane blebs are seen (D and E merged panels, arrows), ANPG disintegrate. (E and F) Proteins abandon the nucleolus and demonstrate a highly irregular distribution in the nucleoplasm; the genomic DNA is condensing to chromatin bodies and partially segregates from the proteins.

Grodno, Belarus, **August 12 - August 24, 2018**

Результаты испытаний МОП транзисторов на воздействие релятивистских частиц

1. Методика экспериментов

Эксперименты проводились на мощных вертикальных полевых транзисторах со структурой металл-окисел-полупроводник, изготовленных в серийном технологическом процессе по технологии двойной диффузии (ДМОП ПТ). Исследовались приборы в пластмассовых корпусах ТО-3Р ($U_{СИ\ макс}$=200 В, $I_С$=30 А, $R_{СИ\ откр}$=0,085 Ом), ТО-220 ($U_{СИ\ макс}$=60 В, $I_С$=50 А, $R_{СИ\ откр}$=0,028 Ом) и металлокерамическом корпусе КТ97С (ТО-258).
При проведении экспериментов приборы располагались в зоне пучка частиц так, чтобы плоскость полупроводникового кристалла, в которой сформирована активная область прибора, была ориентирована перпендикулярно направлению движения частиц. Схема ориентации активной области прибора относительно направления пучка частиц показана на рисунке 1. В процессе экспериментов частицы (дейтроны) попадали на прибор со стороны теплоотвода. Активная область прибора в процессе экспериментов подвергается воздействию, как пучка дейтронов, так и продуктов ядерных реакций, происходящих в окружающей среде при участии дейтронов.

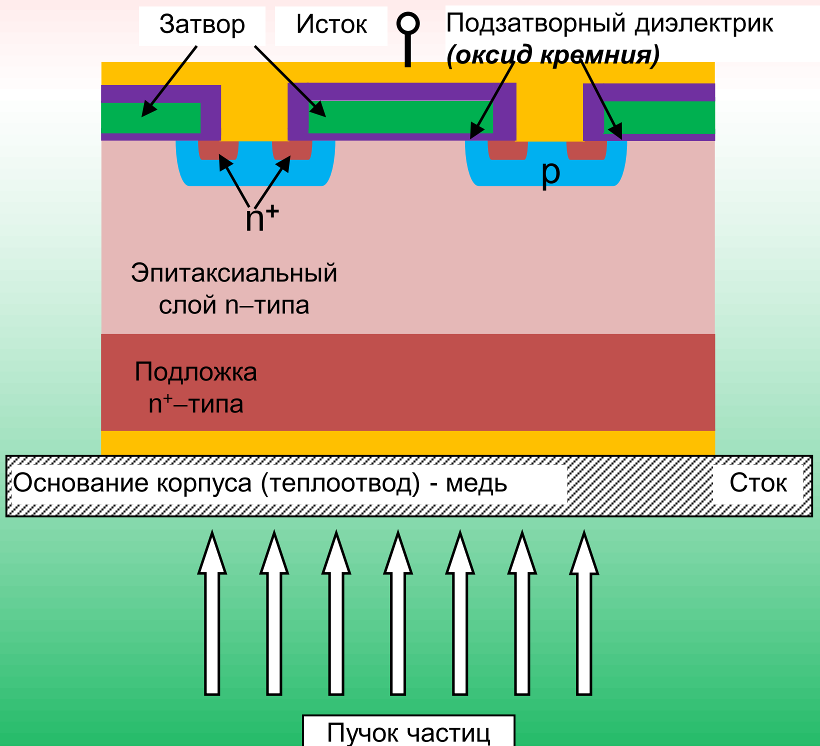

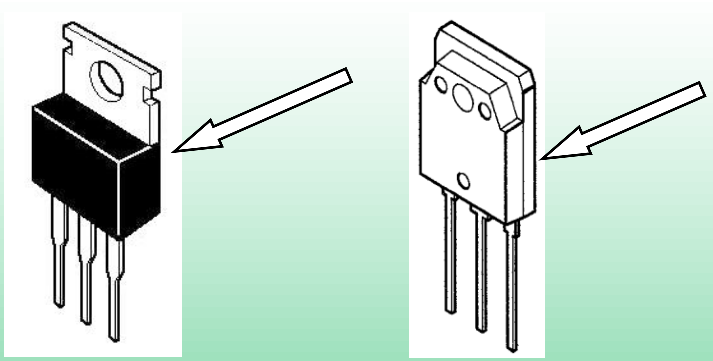

Схема ориентации активной области прибора относительно направления пучка частиц

Результаты по наработке радиоактивных изотопов при облучении транзистора дейтронами с энергией 4 ГэВ (2 ГэВ/нук) приведены в таблице 1 и на рис. а,б,в.
Облучение было начато 13.03.13 в 16-17, закончено 14.03.13 в 01-00.

Наработка радиоактивных изотопов

Изотоп	Тип распада	Период полураспада	Число ядер, наработанное за время облучения	Активность на конец облучения, Бк
Co-57	%EC=100	271.79 d	3.17E+09	94
Ni-57	%EC+%B+=100	35.60 h	3.68E+08	1990
Sc-47	%B-=100	3.3492 d	3.63E+08	869
Sc-48	%B-=100	43.67 h	1.07E+08	472
V-48	%EC+%B+=100	15.9735 d	1.50E+09	754
Co-56	%EC+%B+=100	77.27 d	1.12E+09	116
Sc-44m	%IT=98.80, %EC+%B+=1.20	58.6 h	7.06E+08	2320
Sc-44	%EC+%B+=100	3.927 h	1.13E+08	5540
Cr-48	%EC+%B+=100	21.56 h	2.28E+08	2036
Cr-51	%EC=100	27.7025 d	2.84E+09	823
K-43	%B-=100	22.3 h	1.93E+08	1666
Y-87	%EC+%B+=100	79.8 h	1.68E+08	405
Mn-52	%EC+%B+=100	5.591 d	9.23E+08	1325
Co-58	%EC+%B+=100	70.86 d	3.56E+09	406
Mn-54	%EC+%B+=100, %B-<2.9E-4	312.3 d	3.66E+09	94
Sc-46	%B-=100	83.79 d	9.09E+08	95
Na-24	%B-=100	14.9590 h	7.20E+08	9267
Au-196	%EC+%B+=92.80, %B- =7.20	6.183 d	8.27E+07	107

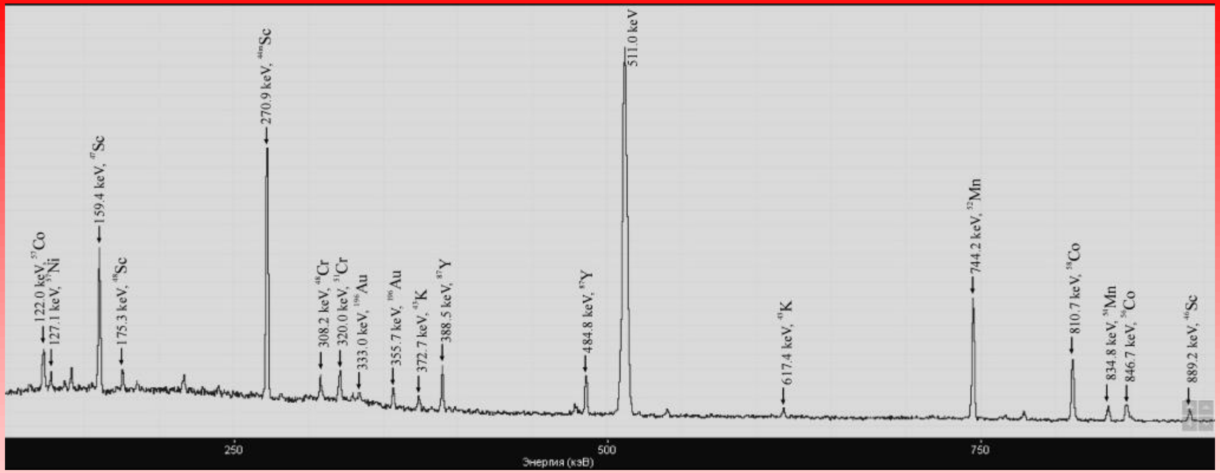

Рис. а

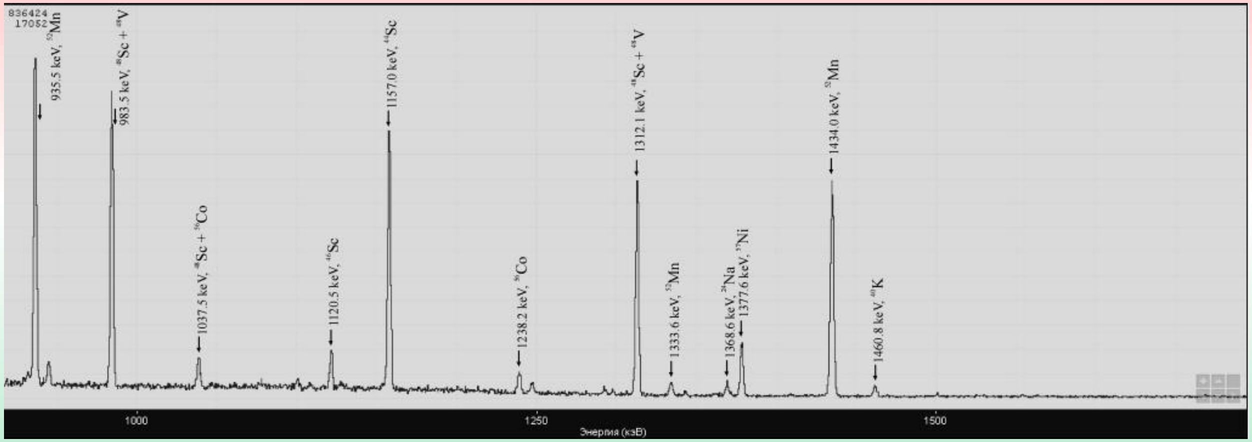

Рис. б

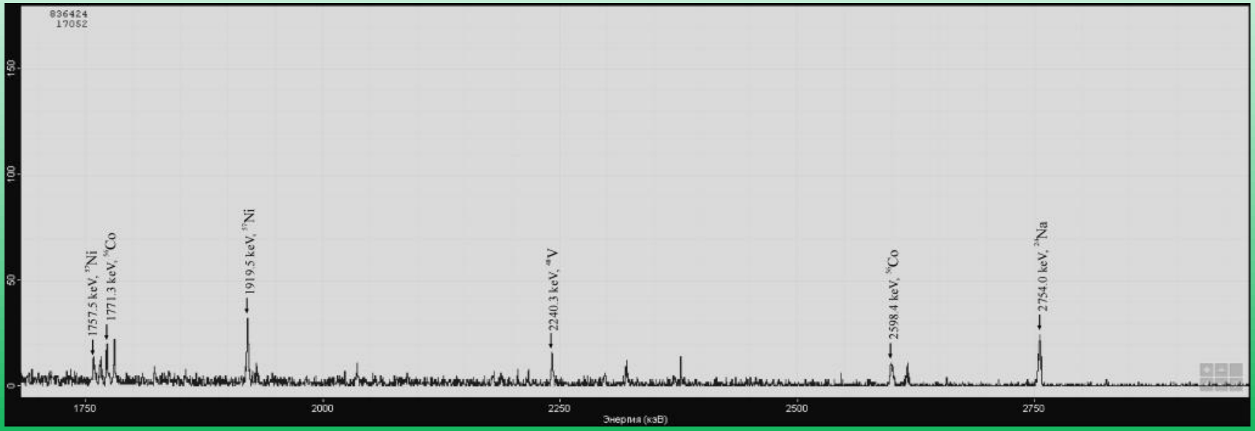

Рис. в

Результаты испытаний МОП транзисторов на воздействие пучком дейтронов

№ эксперимента дата	Количество пакетов импульсов	№ испытываемого транзистора	Корпус	Размер кристалла	Энергия нуклона, ГэВ	Количество нуклонов, Н	Флюенс нуклонов, Н/см^2	Длительность пакета импульсов, сек	Длительность промежутка между пакетами, сек	Скважность	Суммарная энергия нуклонов на кристалл, ГэВ	I_{cu}, нА	$U_{проб}$ В	$U_{пор}$, В	Схема испытаний	Зафиксированный заряд, пКл
1 13.03. 2013	1	63	ТО220	4,32× 4,57	2	$1*10^{10}$	$1,41*10^{9}$	3	12	4	$5,5*10^{8}$	5	60	2,85	рис.1 $U_{пит}$= 10В	
	10					$1*10^{11}$	$1,41*10^{10}$				$5,4*10^{9}$	5	60	2,85		
	100					$1*10^{12}$	$1,41*10^{11}$				$5,4*10^{10}$	5	60	2,85		
	150					$1,5*10^{12}$	$2,12*10^{11}$				$8,1*10^{10}$	5	60	2,85		
2 13.03. 2013	1	51	ТО218	6,53× 6,53	2	$1,4*10^{10}$	$2,04*10^{9}$	3	12	4	$1,74*10^{9}$	5	200	3,28	рис.2 $U_{пит}$= 40В	9550
	10					$1,8*10^{11}$	$2,58*10^{10}$				$1,75*10^{10}$	5	200	3,28		$7,3*10^{4}$
	114					$1,6*10^{12}$	$2,3*10^{11}$				$1,96*10^{11}$	5	200	3,28		$7,4*10^{5}$
3 13.03- 14.03. 2013	1	132	КТ97С	5,8× 7,7	2	$1,4*10^{10}$	$2,04*10^{9}$	3	12	4	$1.74*10^{9}$	5	200	3,2	рис.2 $U_{пит}$= 40В	
	10					$1,85*10^{11}$	$2,64*10^{10}$				$2,25*10^{10}$	5	200	3,2		
	21					$3,7*10^{11}$	$5,3*10^{10}$				$4,7*10^{10}$	5	200	3,2		
4 16.03- 17.03. 2013	1	2	КТ97С	5,8× 7,7	4	$1,82*10^{9}$	$2,6*10^{8}$	1	12	12	$4,64*10^{8}$	10	200	3,2	рис.2 $U_{пит}$= 95В	
	1768					$2,07*10^{12}$	$2,93*10^{11}$				$5,23*10^{11}$	10	200	3,2		